Chapter 8
An Integrated Picture of HDV Ribozyme Catalysis

Barbara L. Golden, Sharon Hammes-Schiffer, Paul R. Carey, and Philip C. Bevilacqua

Abstract The hepatitis delta virus (HDV) ribozyme, a small self-cleaving RNA originally identified in the human pathogen HDV, has been found to be broadly dispersed throughout life. In this article, we describe an integrated approach to understand the catalytic mechanism of this ribozyme that combines kinetics, crystallography, Raman spectroscopy, and calculations. Kinetics studies provide rate and binding parameters for protons and metal ions, and allow for design of properly folded and catalytically relevant RNAs for crystallography. Raman studies on these crystals provide direct evidence that the nucleobase of C75 has a shifted pK_a. Moreover, Raman crystallography and solution kinetics demonstrate that proton binding to the N3 of C75 couples anticooperatively with binding of a Mg^{2+} ion, suggesting that the two species are close in space. Extensive structural studies on this ribozyme suggest that the cleavage reaction proceeds through a combination of Lewis acid catalysis by a catalytic Mg^{2+} ion and general acid catalysis by the nucleobase of C75. Molecular dynamics and electrostatics calculations support the above mechanism and reveal an intensely electronegative pocket that plays key roles in positioning the catalytic metal ion and C75 for catalysis. Integrating the results of kinetics, X-ray crystallography, Raman crystallography, and molecular dynamics suggests that there is a second Mg^{2+} ion in the active site that is bound diffusely and may play a structural role.

B.L. Golden (✉)
Department of Biochemistry, Purdue University,
175 South University Street, West Lafayette, IN 47907, USA
e-mail: barbgolden@purdue.edu

S. Hammes-Schiffer • P.C. Bevilacqua
Department of Chemistry, The Pennsylvania State University,
104 Chemistry Building, University Park, PA 16802, USA
e-mail: shs3@illinois.edu; pcb@chem.psu.edu

P.R. Carey
Department of Biochemistry, Case Western Reserve University,
10900 Euclid Ave, Cleveland, OH 44106, USA
e-mail: prc5@case.edu

R. Russell (ed.), *Biophysics of RNA Folding*, Biophysics for the Life Sciences 3,
DOI 10.1007/978-1-4614-4954-6_8,

In sum, these four disparate approaches provide for a robust kinetic mechanism for the HDV ribozyme that lays groundwork for future studies into its detailed mechanism of dynamics and cleavage.

Keywords Ribozyme • RNA folding • Raman spectroscopy • X-ray crystallography • Molecular dynamics • RNA catalysis

8.1 Introduction

8.1.1 Prelude to HDV: Discovery and Classification of Ribozymes

Until the 1980s it was thought that all enzymes were proteins. The landmark discoveries of Altman and Cech in the early 1980s changed that by demonstrating that naturally occurring RNAs can be catalytic (Kruger et al. 1982; Guerrier-Takada et al. 1983). The RNA enzymes, or ribozymes, , they discovered were RNase P, which is an RNA-protein complex that performs maturation of the 5′-end of tRNA, and the group I intron, which self-splices from a precursor rRNA, mRNA, or tRNA. Although RNase P is an RNA-protein complex, the RNA portion alone is catalytic if a sufficiently high salt concentration is provided to promote folding. Additional ribozymes have been discovered in nature over the ensuing years, including the group II introns and the small nucleolytic ribozymes (hairpin, hammerhead, VS, glmS, and HDV) (Fedor 2009). All of these naturally occurring ribozymes perform RNA cleavage reactions. In addition, numerous RNA and DNA enzymes have been evolved in the laboratory (Ferre-D'Amare 2011). Significant evidence has also accumulated to indicate that both the ribosome and the spliceosome are RNA catalysts (Gong et al. 2011; Klein et al. 2007).

Ribozymes are conveniently separated into two groups: large and small, with the larger ribozymes leaving termini with a 5′-phosphate and 2′,3′-hydroxyl, and the smaller ribozymes leaving 5′-hydroxyl and 2′,3′-cyclic phosphate termini. The HDV ribozymes, which are the focus of this article, are ~85 nt in length and part of the small ribozyme group. The mechanisms of these ribozymes have been studied by many laboratories using multidisciplinary approaches that combine structure, calculations, and functional approaches. The goal of this article is to describe how these disparate approaches have been used together to provide a unified model of the self-cleavage mechanism of the widespread and biologically important catalytic RNA. An emphasis is provided on the collaborative work from our laboratories, especially as it relates to crystallography of the HDV RNA: design and characterization of crystallography constructs to optimize homogeneous folding, growth of crystals under appropriate conditions, Raman crystallography to characterize the ribozyme active site, determination of a crystal structure trapped in the precleavage state, and molecular dynamics calculations on the structure.

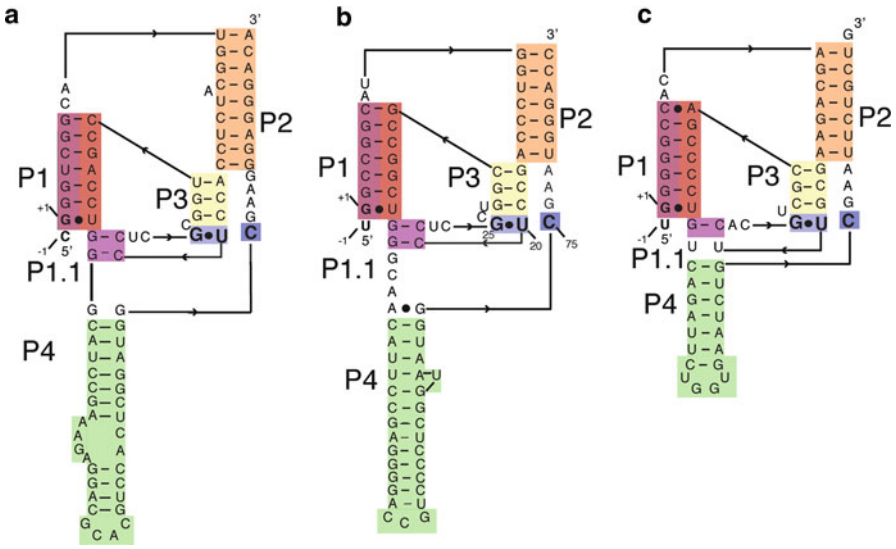

Fig. 8.1 Secondary structures of HDV and HDV-like ribozymes. The antigenomic (**a**), genomic (**b**), and human CBEP3 (**c**) HDV and HDV-like ribozymes have similar secondary structures defined by 5 base-paired regions, P1 (*red*), P1.1 (*violet*), P2 (*orange*), P3 (*yellow*), and P4 (*green*). The G25•U20 reverse wobble and C75 are highlighted in blue; numbering of these features is based on the genomic ribozyme and generally differ for the others

8.1.2 Discovery and Biology of HDV and HDV-Like Ribozymes

The HDV ribozyme was originally discovered as an ~85-nt segment of RNA contained within the 1.7-kb RNA antigenome of the hepatitis delta virus (Sharmeen et al. 1988) (Fig. 8.1). This virus replicates by a double rolling circle mechanism, and the ribozyme self-cleaves to process the resulting concatemers into single-genome-length monomers. The ribozyme is also present in the genomic version of the viral RNA, where it serves a similar role (Kuo et al. 1988; Wu et al. 1989). The genomic and antigenomic ribozymes have similar but non-identical sequences; however, the overall architecture and base pairing are conserved (Fig. 8.1, compare panels A and B). There have been extensive kinetic studies of both the genomic and antigenomic ribozymes, which suggest that the overall structure and mechanism of the two variants are the same (reviewed in (Wadkins and Been 2002). All crystallographic, and therefore computational, studies to date have focused on the genomic ribozyme.

For many years, the HDV ribozyme was believed to be an orphan, without homologs in other organisms. However, there are now many other HDV-like ribozymes known. In an effort to identify ribozymes in the human genome, Szostak and co-workers created a circularized genomic library and used in vitro selection to look for RNA segments that can perform self-cleavage (Salehi-Ashtiani et al. 2006). These studies revealed an active HDV-like ribozyme (Fig. 8.1) contained within an

intron of the *CPEB3* gene (Fig. 8.1c), which encodes a protein believed to regulate mRNA polyadenylation. This study also revealed similar, HDV-like ribozymes in other mammals. In this and a subsequent study, the *CPEB3* HDV-like ribozyme was shown to be similar to the HDV ribozyme in terms of structure, reaction rate, and mechanism (Salehi-Ashtiani et al. 2006; Chadalavada et al. 2010). Although the CPEB3 ribozyme reacts slowly in its native context, this is due to misfolds involving flanking sequence. We demonstrated that when inhibitory interactions of the 5′-flanking sequence are released, the CPEB3 ribozyme reacts much faster, at a rate approaching that of the HDV ribozymes (Chadalavada et al. 2010).

More recent studies driven by structure-based bioinformatics searches have revealed that HDV-like ribozymes are present in diverse organisms, including mosquitoes, plants, and fish. Webb and Luptak have recently described many of these so-called delta-like ribozymes (Webb et al. 2009; Webb and Luptak 2011), and another recent study reported a HDV-like ribozyme at the 5′-termini of R2 elements in *Drosophila*, which is a non-LTR retrotransposon (Eickbush and Eickbush 2010). Although their biological functions are largely unknown, several of these ribozymes, including those in humans and mosquitoes, are active in vivo (Webb et al. 2009). In sum, the wide distribution of these HDV and HDV-like sequences and their diverse functions, from viral genome processing to retrotransposition, heightens the interest in elucidating their underlying molecular mechanisms of self-cleavage activity.

8.1.3 Origins and Evolution of the HDV-Like Ribozymes

The ribozyme from HDV is thought to have arisen from the human CPEB3 ribozyme. Szostak and co-workers have suggested that the absence of HDV isolates from non-human animals implies that the HDV ribozyme arose from the human transcriptome (Salehi-Ashtiani et al. 2006). Interestingly, the only bacterial HDV-like ribozyme currently known is from the human gut bacterium *Faecalibacterium prausnitzii* (Webb and Luptak 2011), suggesting that perhaps this ribozyme was captured from the human genome as well.

At present it is unclear whether the HDV-like ribozymes arose independently multiple times or became dispersed through horizontal gene-transfer events. Luptak and co-workers favor the latter possibility (Webb and Luptak 2011), based in large part upon the inability of random selection experiments to recover HDV-like ribozymes (Wilson and Szostak 1999). Indeed, a HDV-like sequence has never been isolated by in vitro selection experiments, even with pools as diverse as 10^{16} different RNA sequences (Wilson and Szostak 1999). This outcome can be contrasted with that from similar studies on the hammerhead ribozyme, which has been isolated multiple times through in vitro selections (Salehi-Ashtiani and Szostak 2001). (See Chap. 3, for additional discussion on the larger range of RNA topologies in nature compared to those that have arisen in in vitro selection procedures.)

The HDV ribozyme has a remarkably complex fold for a small RNA, including a double pseudoknot (Fig. 8.1). From a statistical point of view, it may thus have

been unlikely for this sequence to arise multiple times. In contrast, the hammerhead core structure consists of just a few simple basepaired stems linked by 13 core nucleotides. Notably, if there was a common ancestor of the HDV ribozyme, the sequence must have mutated extensively through time, as there are only six nucleotides that are known to be conserved among all variants, and the length of these ribozymes can vary from as few as 58 nt (a ribozyme from Pacific abalone that lacks P4) to more than 180 nt owing to various insertions (see below for the nature of insertions) (Webb et al. 2009; Webb and Luptak 2011).

8.2 Conformational Heterogeneity of the HDV Ribozyme

8.2.1 Secondary Structure of the HDV Ribozyme

The native secondary structure of the HDV ribozyme consists of five base-paired regions, P1–P4 and P1.1, and has an overall double-pseudoknotted topology (Fig. 8.1). The P1–P4 secondary-structure elements of the ribozyme were worked out by Been and co-workers in studies using footprinting, site-directed mutagenesis, and self-cleavage approaches (Perrotta and Been 1991). The short, 2 G-C base-pair P1.1 helix was first identified in the crystal structure of the self-cleaved form of the ribozyme (Ferre-D'Amare et al. 1998) and subsequently confirmed by covariation/self-cleavage studies (Wadkins et al. 1999).

Changes in the secondary structure among these HDV-like ribozymes are modest and they generally preserve Watson-Crick base pairing in helices P1–P4 and P1.1. For example, the human CPEB3 ribozyme has only a single base pair in its P1.1 helix (Fig. 8.1c), which is a loss of just one base pair. However, larger variations are known to occur. As in protein enzymes and larger RNA enzymes, such variations in the HDV ribozyme tend to occur at peripheral regions of the molecule or at the sites of bulged nucleotides. Some of these variations can be quite significant. For example, the mosquito *A. gambiae* drz-Agam-2-1 HDV-like ribozyme has two large insertions: a ~40-nt stem-loop insertion in J1/2 and a 68-nt insertion in P4. This ribozyme has been shown to be active both in vitro and in vivo (Webb et al. 2009; Webb and Luptak 2011). The non-effect of these insertions on ribozyme function can be understood in that they are radial extensions away from the core of the ribozyme; they do not add additional pseudoknots or other features that complicate folding. Moreover, they have their own self-structure to allow return of the RNA strand back to the catalytic core at the 3′ end of the insertion.

The first base pair of P1 is critical as it involves the site of the cleavage reaction. In nature, this nucleotide is a purine and is basepaired to a U or a C to form a standard G•U wobble (Fig. 8.1) or a G-C or A-U Watson-Crick base pair. In the genomic HDV ribozyme, this position is tolerant to mutation, with any purine-pyrimidine base pair, including an A•C wobble, being allowed (Cerrone-Szakal et al. 2008). In humans, the CPEB3 ribozyme has a U-to-C single-nucleotide polymorphism (SNP)

that changes the G•U wobble at the base of P1 to a G-C (Vogler et al. 2009). This mutation would be predicted to increase the stability of the P1 helix and has been demonstrated to improve the efficiency of the self-cleavage reaction by 2.6-fold (Salehi-Ashtiani et al. 2006). A behavioral genetic study has linked the higher self-cleavage efficiency of the G-C variant to poor memory performance, presumably due to truncated CPEB3 pre-mRNAs and associated decreased CPEB3 protein expression (Vogler et al. 2009).

8.2.2 The HDV Ribozyme Is Subject to Misfolding

The folding of the HDV ribozyme is stimulated by partially denaturing conditions, including semi-denaturing conditions of 5 M urea or 10 M formamide (Rosenstein and Been 1990; Smith and Dinter-Gottlieb 1991). This odd behavior is due in large part to the G-C-rich nature of the pairings. This leads to a melting temperature of >70 °C for the tertiary structure in physiological Mg^{2+} concentrations (Nakano et al. 2003). In addition, the complex topology conferred by the presence of two pseudoknots complicates folding. The difficulty in folding due to the pseudoknots can be understood by considering the folding pathway. For example, in principle during cotranscriptional folding, the 5′ strand of P2 should "wait" for the 3′ strand of P2 to be synthesized before it engages in pairing. However, the two strands of P2 are separated by a large stretch of sequence, 62 nt in the genomic ribozyme (Fig. 8.1b). As such, before P2 can form, the six nucleotides that make up the 5′ strand of P2 are likely to engage in alternative base-pairings that can interfere with folding. Numerous such alternative pairings in the folding pathway of the ribozyme have been identified, and these must melt to allow proper folding of the genome. Indeed, the rate at which the HDV ribozyme folds to its native conformation is dominated by slow folding of the secondary structure into a pseudoknotted topology and it is likely that denaturants accelerate catalysis by facilitating this transition (Chadalavada et al. 2000, 2002; Brown et al. 2004).

Computational work from Isambert and Siggia suggested that non-native interactions formed by the 5′ strand of P2 could in fact *aid* folding along the cotranscriptional folding pathway, and they dubbed such interactions "folding guides" (Isambert and Siggia 2000). Our experimental mutational studies provided some support for this notion, although we ultimately obtained the fastest folders, at least for RNAs refolded from traditional denaturing PAGE purifications, using mutations that disrupted all possible alternative pairings (see next subsection) (Brown et al. 2004). Nonetheless, it is noteworthy that the wild-type sequence of the genomic HDV ribozyme was found to be the optimal sequence under cotranscriptional folding conditions (Chadalavada et al. 2007), supporting the notion of unique pathways for cotranscriptional folding of the RNA—conditions under which it evolved to self-cleave, perhaps utilizing the folding guides in ways that have yet to be fully elucidated.

8.2.3 *Analysis of Structural Heterogeneity and Preparation of Homogeneous Systems for Biophysical Analysis*

While self-cleavage activity of the genomic HDV ribozyme is stimulated by partially denaturing conditions, it is inhibited by fully denaturing conditions such as 9.5 M urea or 22.5 M formamide (Rosenstein and Been 1990). The inhibition of reactivity by fully denaturing conditions is suggestive of requirement of a native ribozyme secondary structure for reactivity, while the stimulation of activity under semi-denaturing conditions is suggestive that this native structure is frustrated by misfolding. When we began studying the HDV ribozymes, we attempted to identify misfolds of the ribozyme and to "fix" them by making mutations that disrupted the alternative folds while retaining the five native double-helices. We reasoned that use of a native folding ribozyme would simplify behavior in biophysical and biochemical experiments and possibly aid efforts to crystallize the RNA in a native state.

There are two general classes of non-native folds in the ribozyme that one can consider: those involving base pairing between the ribozyme and flanking RNAs, and those involving base pairing within the ribozyme sequence. The upstream sequence of the genomic HDV ribozyme has the potential to base pair to the 3′ strand of P2. This misfolded helix is called Alt 1 (Chadalavada et al. 2000). The Alt 1 pairing can be destabilized by mutation, by deletion, or by antisense oligonucleotides that basepair to the upstream interfering sequence. These strategies rescue self-cleavage activity by a remarkable 2,000- to 20,000-fold by accelerating folding to the native state. The human CPEB3 ribozyme also contains an alternative pairing between upstream sequence and the ribozyme that when removed rescues self-cleavage, in this case by 250-fold (Chadalavada et al. 2010).

The second class of non-native folds, those involving ribozyme-ribozyme interactions, is extensive and complex in the genomic HDV ribozyme. We identified and named five such alternative helices (Fig. 8.2). Alt P1, Alt 2, and Alt 3 are relatively simple, stable helices that differ from those found in the native structure. Alt X and Alt Y involve two GGG sequences capable of stable base-pairing with five- and seven-nucleotide polypyrimidine stretches (Brown et al. 2004). The sequence degeneracy in these regions means that the Alt X and Alt Y misfolds can include several alternative registers.

We tested over 20 different sequences containing one to five mutations relative to wild type for their ability to lead to more native folding. This characteristic was judged by an increase in the rate constant for self-cleavage, the extent of self-cleavage, and by the ability to fit the data to a single exponential. We ultimately identified a variant with the desired properties, in which G11 is mutated to a C, and the nonconserved nucleotide U27 is deleted (G11C/U27Δ) (Brown et al. 2004). In this double mutant, Alt P1 is weakened by the G11C mutation, and Alt 3 is weakened by the deletion of U27. The G11C/U27Δ ribozyme reacts monophasically and to completion with the rapid rate constant of 1 s^{-1}. This rate constant likely corresponds to the intrinsic rate of ribozyme cleavage (Emilsson et al. 2003). We thus reasoned that the G11C/U27Δ variant might be well disposed to native folding and based our crystallography constructs upon it (Fig. 8.3).

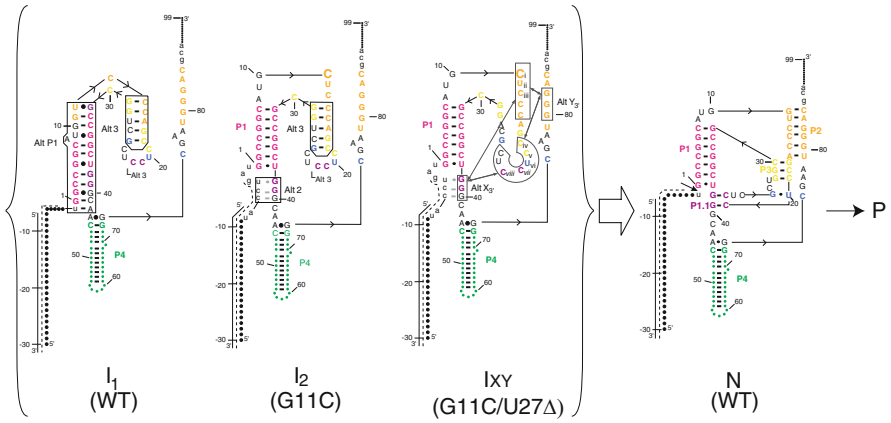

Fig. 8.2 Alternate secondary structures accessible by the genomic HDV ribozyme. Nucleotides are colored to correspond to their native secondary structures as in Fig. 8.1: P1 (*red*), P1.1 (violet), P2 (*orange*), P3 (*yellow*), and P4 (*green*). The G25•U20 reverse wobble and C75 are highlighted in blue. Figure adapted from (Brown et al. 2004) with permission

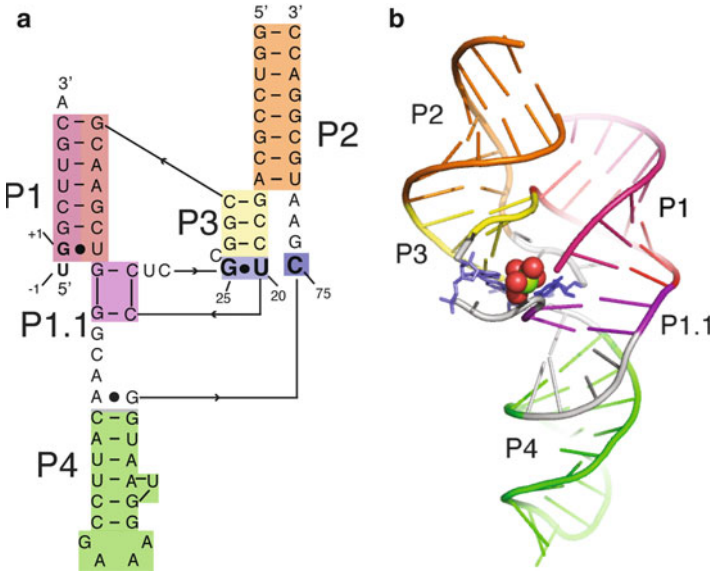

Fig. 8.3 Secondary (**a**) and tertiary (**b**) structures of a trans-acting HDV ribozyme. This sequence is based on the homogeneously folding G11C/U27Δ variant. In both panels, the helices are colored according to the following scheme: P1 (substrate strand-*magenta*, ribozyme strand-*red*), P1.1 (*violet*), P2 (*orange*), P3 (*yellow*), and P4 (*green*). The G25•U20 reverse wobble and C75 are highlighted in *blue* and are shown as sticks in panel b. The catalytic Mg^{2+} ion and its hydration shell observed in pdbid 3NKB are drawn as spheres. Figure adapted from (Chen et al. 2010) with permission

8.3 Three-Dimensional Structure of the HDV Ribozyme

8.3.1 The Structure of the Ribozyme Pre- and Postcleavage Is Similar

The crystal structure of the HDV ribozyme was initially determined in 1998 by Ferré-D'Amaré et al., in the self-cleaved form (Ferre-D'Amare et al. 1998). Two strategies were used to overcome the conformational heterogeneity intrinsic to this ribozyme. First, a binding site for the protein U1A was introduced into the L4 loop of the ribozyme (Ferre-D'Amare et al. 1998; Ferre-D'Amare and Doudna 2000). Binding of U1A protein to L4 stabilizes the native secondary structure and drives the reaction toward the folded conformation. The U1A protein-RNA complex also adds chemical diversity over that present in RNA alone, which provides additional possibilities for crystal contacts and thereby aids crystallization of the ribozyme. Second, prior to crystallization the self-cleaved ribozyme was isolated on a gel that allowed the RNA to retain native structure (Ferre-D'Amare and Doudna 2000). This ensured that only RNAs capable of accurate cleavage were present in the crystallization experiments. This provided a snapshot of the HDV ribozyme post-cleavage that has turned out to be consistent with extensive experimentation.

To obtain structural information on the ribozyme *prior* to cleavage, it is necessary to trap the ribozyme in the precleavage state by inhibiting the reaction in some manner. This is a critical issue, because the goal is to inhibit the reaction while preserving the network of native interactions in the active site. A common means of capturing ribozymes in a catalytically inactive, but biologically relevant conformation is to modify the 2′-hydroxyl nucleophile to prevent attack at the scissile phosphate (Rupert and Ferre-D'Amare 2001; Cochrane et al. 2007; Martick and Scott 2006; Klein and Ferre-D'Amare 2006). In the case of the HDV ribozyme, a 2′-deoxy or 2′-methoxy substitution was introduced at U(−1) to create a noncleavable substrate analog. To use this modification, it was necessary to separate the cleavage site from the ribozyme because the HDV ribozyme is too large for complete chemical synthesis. In the case of the HDV ribozyme, this was readily accomplished by introducing a break between the P1 and P2 helices (Fig. 8.3). The 5′-strand of P1 was then added back in trans to the ribozyme body, which was produced by in vitro transcription, to reconstitute the ribozyme via strong G-C-rich base pairing. To reduce the conformational heterogeneity and to facilitate crystallization, the homogeneously folding G11C/U27Δ mutant was used.

We solved the structure of the 2′-deoxy-inhibited ribozyme at 1.9 Å by X-ray crystallography (Chen et al. 2010) (Fig. 8.3). This provided a look at the HDV ribozyme active site at unprecedented resolution; however, the cleavage site dinucleotide was partially disordered. To create a snapshot of the ribozyme prior to reaction, the cleavage site of the hammerhead ribozyme was modeled into the active site of the HDV ribozyme using the position of G1 as a guide (Chen et al. 2010). Comparison of the electron density maps with the resulting model suggests that this approach is valid. In particular, there is 3σ electron density for the scissile phosphate, unbroken

density for the cleavage site at 0.5σ, and density for the nucleobase of U(−1); also, the model was consistent with a wealth of biochemical data (see below).

8.3.2 Structure of the Active Site

A number of key interactions can be found in the ribozyme active site that serve to position the substrate and facilitate catalysis (Fig. 8.4).

8.3.2.1 In Both the Post- and Precleavage Crystal Structures, C75 Interacts with the 5′-Oxygen Leaving Group

In the postcleavage structure, the N3 of C75 is a hydrogen bond acceptor, and the 5′-hydroxyl group of G1 is the hydrogen bond donor. This interaction is maintained in the ribozyme precleavage state, as the N3 of C75 is again within hydrogen-bonding distance (~3.6 Å) of the 5′-oxo group of G1 (Fig. 8.4a). To maintain the hydrogen bond prior to cleavage, the N3 of C75 must be a hydrogen bond donor, as the 5′-oxygen of G1 is not linked to a hydrogen atom and so must be a hydrogen bond acceptor. The presence of this hydrogen bond in the trapped precleavage state suggests that the nucleobase of C75 is protonated and thus positively charged prior to cleavage. This is consistent with the fact that the crystal structure was solved at a pH of 5.0, which is below the pK_a of C75.

8.3.2.2 In the Precleavage Crystal Structure, a Rare Reverse G•U Wobble Base Pair Forms Between G25 and U20

In the structure of the HDV ribozyme prior to substrate cleavage, G25 is in the rare *syn* conformation, and it forms a base pair with U20 in a geometry referred to as a "reverse wobble" conformation (Fig. 8.4b). In the structure of the ribozyme in the postcleavage state, G25 and U20 are near each other, although the optimal reverse wobble geometry was not observed. However, re-examination of the diffraction data along with molecular dynamics (MD) simulations (discussed below) suggested that the G25•U20 reverse wobble is in fact maintained after the cleavage event (Krasovska et al. 2005; Veeraraghavan et al. 2010, 2011a).

The G25•U20 reverse wobble pair in the precleavage structure coordinates an Mg^{2+} ion through its hydration shell and thereby helps position it within the active site (Fig. 8.4b). The interaction between the G25•U20 reverse wobble and the Mg^{2+} ion is reminiscent of the interaction between hydrated metal ions and standard G•U wobble pairs. However, while a standard G•U wobble pair positions hydrated Mg^{2+} ions in the deep cleft of the major groove, the reverse wobble places the Mg^{2+} ion in the minor groove where it can make long-range interactions with other nucleotides from the ribozyme.

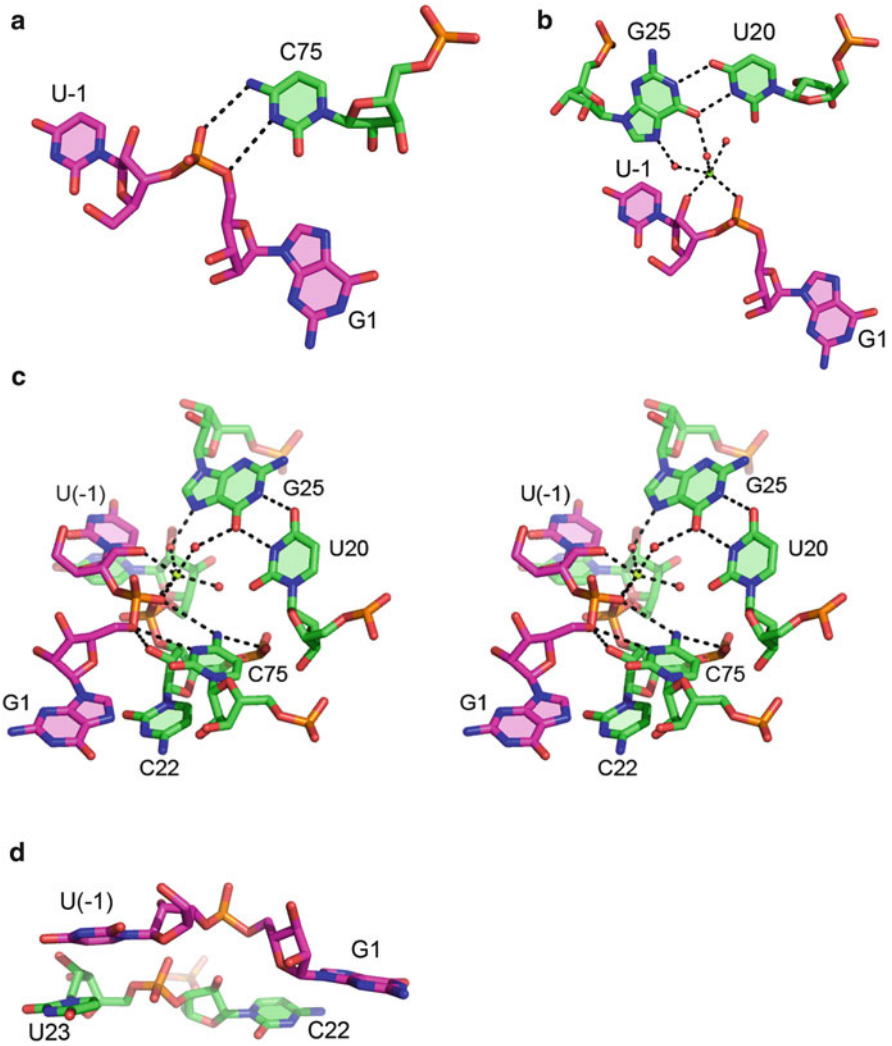

Fig. 8.4 Interactions observed in the active site of the HDV ribozyme. (**a**) C75 interacts with the 5′-O and pro-R_p oxygen of G1. These interactions likely help to raise the pKa of the N3 of C75 and position the nucleobase for general acid catalysis. (**b**) The G25•U20 reverse wobble helps position the catalytic metal ion to interact with the 2′-hydroxyl of U(−1) and the pro-R_p oxygen of G1. (**c**) Stereoview of the active site highlighting the network of hydrogen bonds and Mg^{2+}-facilitated interactions that position C75 and the cleavage site dinucleotide. (**d**) Spatial relationship of the cleavage site dinucleotide with C22 and U23. The U(−1) nucleobase stacks on U23 but does not form hydrogen bonds, consistent with lack of specificity in the identity of the nucleobase at (−1)

8.3.2.3 An Mg^{2+} Ion in the Active Site Interacts Directly with the Cleavage Site

In the model of the ribozyme in the precleavage state, the metal ion is positioned to make direct contacts with the 2′-hydroxyl group of U(−1) and the pro-R_p oxygen of the scissile phosphate (Fig. 8.4b). Substitution of the pro-R_p oxygen with a sulfur atom gives only ~10% reaction product (Fauzi et al. 1997). As sulfur is bulkier and interacts less strongly with Mg^{2+}, this result suggests the importance of the interaction of this position with the active site Mg^{2+} ion. Coordination of the cleavage site dinucleotide in this fashion serves to position the 2′-hydroxyl group for in-line attack at the scissile phosphate.

The interaction between the cleavage site dinucleotide and the active site Mg^{2+} ion is reminiscent of the metal ion interactions observed in the active sites of large ribozymes that splice or cleave RNAs. In group I and group II introns and RNase P, a pair of Mg^{2+} ions interact with the scissile phosphate, the nucleophile, and the leaving group (Adams et al. 2004; Guo et al. 2004; Golden et al. 2005; Toor et al. 2008; Reiter et al. 2010; Frederiksen and Piccirilli 2009). These two-metal ion mechanisms are similar to those observed in RNA and DNA polymerases (Steitz and Steitz 1993). The metal ions facilitate catalysis by activating nucleophiles, stabilizing leaving groups, and organizing the substrate RNAs into conformations consistent with cleavage. The location of the Mg^{2+} ion in the HDV ribozyme active site suggests that this ribozyme, like its much larger cousins, is a metalloenzyme. This active site Mg^{2+} ion will be referred to hereafter as the "catalytic Mg^{2+} ion".

8.3.2.4 An Intricate Network of Hydrogen Bonds Positions the Substrate Within the Active Site

C75 is held in position by interactions between its exocyclic amine (N4) and the phosphate groups from nucleotides 1 and 23 (Fig. 8.4c). The importance of these interactions is underscored by the catalytic and structural consequences of deleting the exocyclic amine or making a substitution at position 75; substitution of C75 with A impairs catalytic activity, while substitution with U eliminates catalytic activity (Perrotta et al. 1999). The structure of the HDV ribozyme harboring the C75U mutation reveals an active site that is significantly rearranged and distorted from the WT postcleavage and precleavage structures (Ke et al. 2004).

The cleavage site dinucleotide consists of U(−1) upstream of the scissile phosphate and G1 downstream of the scissile phosphate. The position of the downstream nucleobase is defined by basepairing with the pyrimidine at position 37 to form a standard Watson-Crick or wobble base pair at the base of the P1 helix (Cerrone-Szakal et al. 2008). The position of the backbone at G1 is defined by its interactions with C75, which interacts with both the 5′-oxygen (hydrogen bond to C75N3) and pro-R_p oxygen (hydrogen bond to C75N4) of G1 (Fig. 8.4a). The 2′-hydroxyl group of C22 is also within hydrogen-bonding distance of the 5′-oxygen and pro-R_p oxygen of G1 (Fig. 8.4c). The catalytic Mg^{2+} orients the 2′-hydroxyl of U(−1) and the

pro-R_p oxygen of G1 (Fig. 8.4b). In addition, the 2′-hydroxyl of U(−1) is in hydrogen-bonding distance of the 2′-hydroxyl of G27 (2.9 Å, not shown in Fig. 8.4) and one of the water molecules coordinated to the active site Mg^{2+} (3.1 Å). In summary, all of the key hydrogen-bonding partners in the backbone of the cleavage site dinucleotide are involved in multiple hydrogen or metal-mediated bonds (Fig. 8.4c). These interactions serve to stabilize the cleavage site in a conformation poised for in-line attack of the 2′-hydroxyl at the scissile phosphate.

8.3.2.5 The Nucleobase of U(–1) Stacks on the Bulged Base U23

The nucleotides upstream of the cleavage site are not known to base pair, and there is no sequence requirement for these nucleotides. Moreover, after cleavage, the upstream cleavage product dissociates rapidly. Thus, although the reverse reaction of ligation is chemically favorable and observed in most other small ribozymes, it is not observed in the HDV ribozyme. In the model of the precleavage ribozyme, U(−1) is stacked upon U23 (Fig. 8.4d), but there are no hydrogen bonds to the U(−1) nucleobase. This stacking interaction is supported by data that suggest that RNAs containing purines at the −1 position bind tighter to the ribozyme (Shih and Been 2001a). Thus, stacking at U(−1) without base pairing appears to help orient this nucleotide for catalysis, while still allowing U(−1) and the upstream RNA to dissociate rapidly after cleavage. This has biological implications, as cellular functions that employ the HDV and HDV-like ribozymes must be tolerant of or gain an advantage from the irreversibility of the reaction; indeed, HDV appears to employ a host factor to drive ligation of linear product pieces when needed (Reid and Lazinski 2000).

8.4 Raman Crystallography of the HDV Ribozyme

8.4.1 Use of Raman Crystallography to Characterize the HDV Ribozyme Active Site

Raman crystallography refers to recording the Raman spectrum of a macromolecular single crystal by using an optical microscope coupled to a Raman spectrometer. The spectrum can be obtained in tens of seconds, which allows chemical changes occurring inside the crystal to be followed. The crystal is maintained in a hanging drop within a well of a standard crystallization tray under ambient conditions. Because the crystal is not frozen, conformational changes can occur and be observed. The solution conditions in the hanging drop are changed by the addition of buffers at different pH, or a metal, or a substrate for an enzyme. The “small molecule” penetrates the crystal and by recording the Raman spectrum, events inside the crystal can be probed. Normally the changes are detected by subtracting the initial spectrum of the crystal from that of the crystal after adding the reactant. Technical details of these experiments are available (Carey 2006; Gong et al. 2007, 2009b; Long 2002).

Raman crystallography has been used to characterize interactions within the active site of the HDV ribozyme and to verify that the crystallized ribozyme has properties similar to the ribozyme in solution (Gong et al. 2007, 2008, 2009a; Chen et al. 2009). In this section, we focus on two issues directly relevant to the ribozyme: proton and metal binding to the ribozyme. The major workhorse in the Raman analysis is the spectrum of the HDV crystal. To set the scene, this is shown in Fig. 8.5, and peak assignments based on an extensive literature are given in Table 8.1 (Carey 1982; Thomas and Tsuboi 1993; Gong et al. 2007).

8.4.2 Measurement of Proton Binding to the HDV Ribozyme by Raman Crystallography

Because RNA is built from only four similar nucleotides, peaks in RNA Raman spectra are highly overlapped. Quantitating changes in the Raman signature of a single active site residue as a function of pH is therefore a major challenge. A spectral feature near 1,530 cm^{-1} in the Raman spectrum of the HDV ribozyme crystal provides a key. As can be seen in Fig. 8.5 this is intrinsically a "weak" feature, and band fitting seen in Fig. 8.6 reveals a further complication—the band profile is made up of two components. One feature, near 1,536 cm^{-1}, is due to a guanine ring mode, and the second, near 1,528 cm^{-1}, is assigned to the ring mode of a neutral, unprotonated cytosine. Its intensity at pH 8.5, where all free cytosines are neutral, is equivalent to a single cytosine in the ribozyme. To test the hypothesis that this feature arises from the key active site residue C75, we crystallized and acquired spectra from the ribozyme variant C75U. These spectra lacked the 1,528 cm^{-1} component as predicted. Thus, by plotting the intensity of the 1,528 cm^{-1} component as a function of pH we could obtain the pK_a of C75. In this way, we determined that the pK_a of C75 in the presence of 20 mM Mg^{2+} is 6.15 ± 0.08, shifted more than two pH units higher than that of free cytosine in solution. When the concentration of Mg^{2+} is reduced to 2 mM, the pK_a of C75 shifted further upward, to 6.40 ± 0.05. Thus, the pK_a of C75 couples anticooperatively with Mg^{2+} concentration, in excellent agreement with biochemical experiments performed in solution.

Two conclusions can be drawn from this set of experimental results. First, cytosine C75 has a pK_a value that is dramatically shifted by its environment within the ribozyme active site. While the HDV ribozyme was the first ribozyme to reveal an active site component with a shifted pK_a, later studies revealed that the pK_as of adenine 38 in the hairpin ribozyme (Guo et al. 2009) and the glucosamine-6-phosphate co-factor amine bound to the glmS ribozyme (Gong et al. 2011) are also shifted toward neutrality. Second, binding of the proton on C75 is anticooperative with respect to binding of an Mg^{2+} ion, giving the observed dependence of pK_a on Mg^{2+} concentration. This result suggests that there is an Mg^{2+} ion in the active site near C75, such that the two cations can sense each other electrostatically and that this phenomenon can be observed by Raman spectroscopy (discussed below).

Table 8.1 Wavenumbers (cm^{-1}) and assignment of major raman bands observed in Raman spectrum of HDV Ribozyme Crystal

Wavenumber	Assignment
1,677 (m)	Base C=O
1,574 (s)	A, G
1,535 (w)	G
1,528 (w)	C
1,483 (vs)	G, A
1,460 (w)	C-H (ring)
1,421 (w)	A, G
1,376 (m)	A, G
1,337 (s)	A
1,322 (s)	G
1,252 (s)	C
1,232 (sh)	U
1,181 (w)	G
1,101 (s)	PO_2^-
1,045 (w)	Ribose
999 (w)	Ribose
917 (w)	Ribose
812 (s)	
784 (vs)	C, U
725 (m)	A
670 (m)	G
633 (w)	G

Vs very strong, *s* strong, *m* medium, *w* weak, *sh* shoulder. The features assigned to the bases are due to ring modes

8.4.3 Measurement of Metal Ion Binding to the HDV Ribozyme by Raman Crystallography

Metal cation-RNA interactions can be of pivotal importance in RNA folding and RNA-catalyzed reactions (Feig and Uhlenbeck 1999). The potential for using Raman spectroscopy to probe for metal-nucleic acid interactions has been appreciated for some time (Mansy et al. 1978; Duguid et al. 1993; Christian et al. 2010; Moller et al. 1980) (and references therein), and now the HDV ribozyme has furnished a case wherein inner sphere metal-RNA contacts have been detected directly by Raman in single crystals of a large RNA (Gong et al. 2008). To remove divalent cations, a HDV crystal is treated extensively and multiple times with an EDTA solution, leaving only monovalent cations in the crystal. Mg^{2+} is then soaked into the crystal, and difference spectra calculated [Raman HDV + Mg^{2+}] minus [Raman HDV no Mg^{2+}]. As seen in Fig. 8.7 there are two regions of note: the differential around 1,100 cm^{-1} is due to stretching motions of the backbone PO_2^- groups and can also be observed in the parental spectrum (1,101 cm^{-1} in Fig. 8.5). In the subtraction process, a few phosphates make direct contact with metal ions. The PO_2^- modes corresponding to

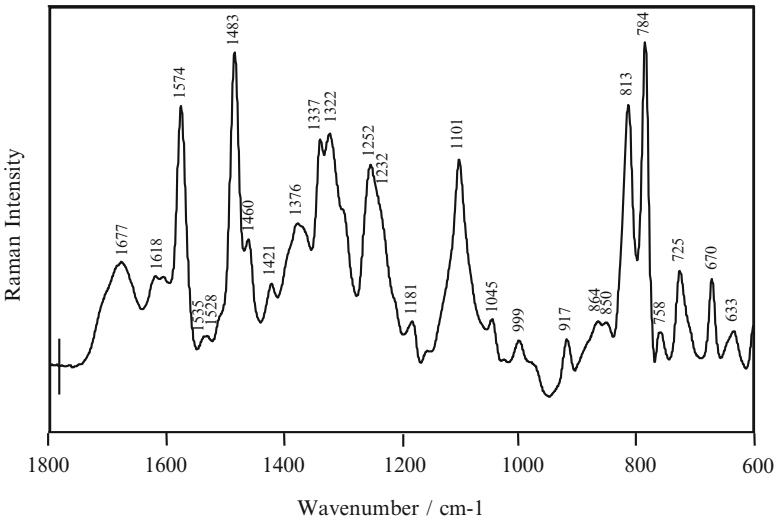

Fig. 8.5 Raman spectrum of a WT HDV ribozyme crystal inhibited by a 2′-methoxy substitution at U(−1). The vertical bar represents a 5,000 photon event. Peak assignments are listed in Table 8.1. Figure from (Gong et al. 2007) and used with permission

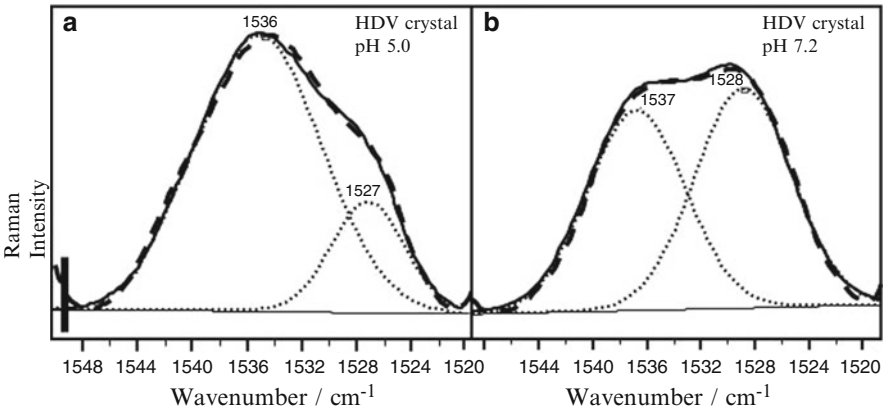

Fig. 8.6 Curve fitting of the cytosine band of a HDV crystal at low and high pH. The feature at 1,527/1,528 cm^{-1} is due to neutral cytosine, assigned to C75 based on mutants, and is used to derive the pK_a for this active site residue. The overlapping band at 1,536/1,537 cm^{-1} is due to a guanine ring mode. As the pH is increased from 5.8 to 8.2, the band at 1528^{-1} increases in proportion to the concentration of neutral cytosine. Figure from (Gong et al. 2007) and used with permission

these nucleotides are upshifted to 1,117 cm^{-1} by their contact with Mg^{2+} ions. This creates the upper limb of the differential, while the negative limb is due to the same PO_2^- groups removed from the population of free, unliganded PO_2^- groups (Fig. 8.7a).

The Mg^{2+} ions directly coordinated to these phosphate groups can also be detected in the spectra. These are observed near 322 cm^{-1} (Fig. 8.7b). The extensive physicochemical analyses of these species carried out by Peleg (1972) and Pye and Rudolph

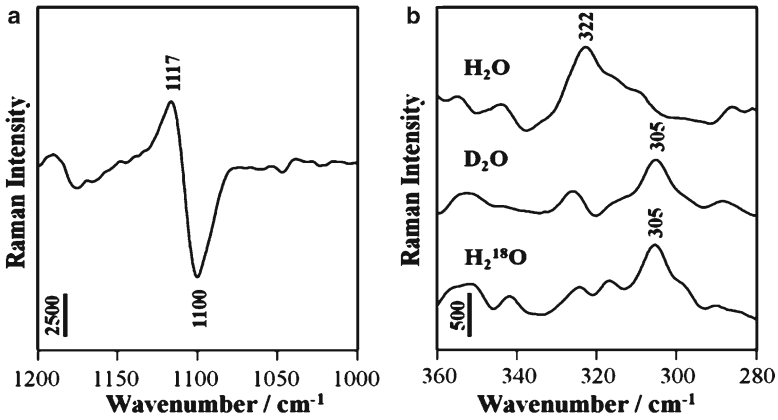

Fig. 8.7 Partial Raman difference spectra of HDV crystals [HDV + 20 mM Mg^{2+}] minus [HDV without Mg^{2+}] at pH 6.0, vertical bars are photon events. (**a**) Symmetric stretch of PO_2^- groups bind inner sphere to Mg^{2+} at 1,117 cm^{-1}; the negative node at 1,100 cm^{-1} is due the mode from metal-free groups. (**b**) Raman signatures of Mg hydrate (pentahydrate and tetrahydrate are both possible) bind inner sphere to PO_2^- oxygen, showing isotope shifts. Figure from (Gong et al. 2008) and used with permission

(1998) suggest that this feature corresponds to Mg^{2+} penta- and/or tetra-hydrate. This band is downshifted in the expected manner upon D_2O or H_2O^{18} substitution (Fig. 8.7b). The ratio of the increasing 1,100 (differential) and 322 cm^{-1} intensities remains constant over the range 5–40 mM Mg^{2+}, suggesting a 1:1 correspondence between the perturbed PO_2^- population and the creation of the penta-hydrate species. This key finding implies that there is likely inner sphere contact wherein the Mg^{2+} atoms are in direct contact with the PO_2^- group. At 20 mM Mg^{2+}, the intensity of the negative 1,100 cm^{-1} limb in Fig. 8.7a compared to the intensity of the "total" PO_2^- band in the parental spectrum near 1,100 cm^{-1} (Fig. 8.5) suggests that about five PO_2^- groups are in inner sphere contact with Mg^{2+} ions. This agrees well with the four Mg^{2+} ions observed to make inner sphere contacts to RNA in our recent X-ray crystal structure of a similar construct (Chen et al. 2010). However, there is a notable difference between evaluations using X-ray and Raman analyses. The X-ray approach only reveals Mg^{2+} ions at binding sites that have sufficient occupancy to create detectable electron density. The positive limb of the differential in Fig. 8.7a will have contributions from these sites but will also have contributions from transient PO_2^-—$Mg(H_2O)_5^{2+}$ inner sphere complexes at multiple PO_2^- sites in the ribozyme. The latter, while unobservable by X-ray diffraction, will add intensity to the negative differential.

8.4.4 Dependence of Metal Binding on N7 of G1

Most Mg^{2+} binding sites in RNA are insensitive to pH in the range from 4 to 9; however, protonation of C75 has the potential to affect binding of Mg^{2+} ions within the

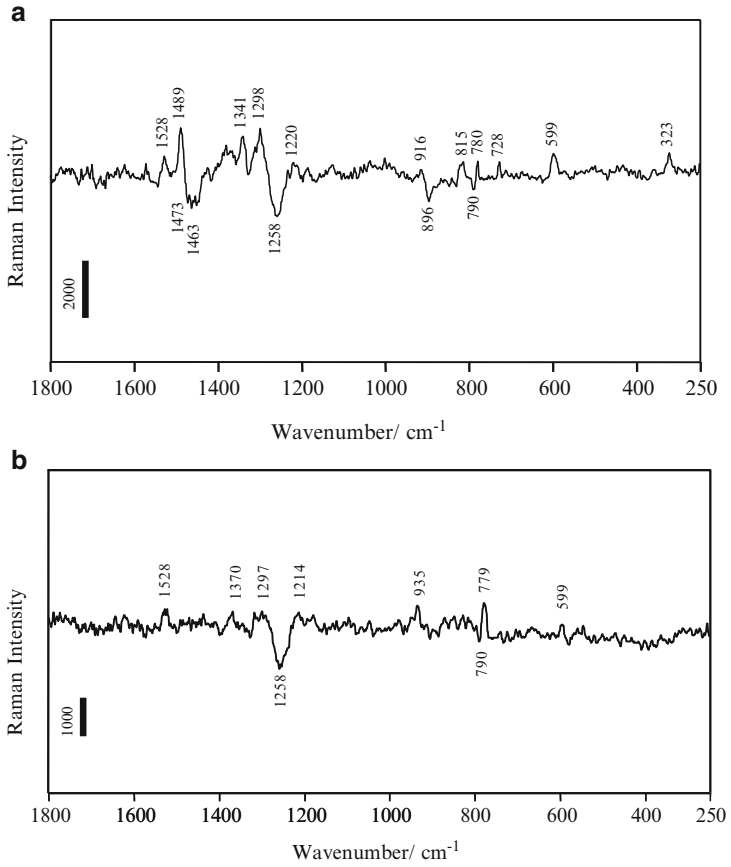

Fig. 8.8 Raman difference spectra of (**a**) [HDV crystal pH 7.5] minus [HDV crystal pH 5.0]. (**b**) Same as panel A but with 7-deazaG1 where at residue G1 the N atom at position 7 on the guanine ring is replaced by CH. Figure from (Chen et al. 2009) and used with permission

ribozyme active site. Indeed, changes in Mg^{2+} binding to the HDV ribozyme can be observed by comparing the Raman spectra as a function of pH (Chen et al. 2009). The positive and negative features in Fig. 8.8 represent the changes in the parent Raman spectrum with an increase in pH. Positive peaks are from HDV groups that are present at pH 7.5 but absent at pH 5.0, and negative peaks vice versa. The peak assignments can be made using Table 8.1. In addition to the peak at 1,528 cm^{-1} arising from neutral cytosine (C75), a feature at 322 cm^{-1} in Figs. 8.7b and 8.8 is observed. This feature corresponds to a single hydrated Mg^{2+} ion with at least one non-water ligand that is lost upon protonation of C75. Quantitation of intensities reveals that there is one Mg^{2+} hydrate lost per HDV ribozyme. As the nucleobase of C75 is the only functional group in the ribozyme that has a pK_a in this range, we infer that the lost Mg^{2+} hydrate

is bound near the active site, although it could be linked by an allosteric change. This metal ion does not appear to be the catalytic Mg^{2+} ion, because it is not bound by a phosphate group, as there is no evidence for a corresponding "PO_2^-—inflection" near 1,100 cm^{-1} in Fig. 8.8. In contrast, the catalytic Mg^{2+} ion is liganded by both the scissile phosphate and phosphate group of U23. The catalytic Mg^{2+} ion is bound in a highly electronegative patch within the ribozyme active site and may be bound with sufficient affinity to withstand protonation of the neighboring C75 under the conditions of these experiments (Chen et al. 2009). Such a scenario would be consistent with a concerted reaction mechanism involving simultaneous presence of Mg^{2+} and $C75^+$, as suggested by recent calculations (Ganguly et al. 2011).

The 1,489/1,473 cm^{-1} inflection in Fig. 8.8a suggests that a guanosine base may be perturbed by the loss of the Mg^{2+} hydrate. There are few guanosine bases near the active site; however, G1, the nucleotide at the cleavage site, could potentially interact with this Mg^{2+} hydrate. Consistent with this, it was found that when G1 was replaced by 7-deazaguanosine, which replaces the purine's N7 with a methine group (CH), Raman signatures for the ejected Mg^{2+} ion and its ligand were lost (Fig. 8.8b). Substitution of G1 with 7-deazaguanosine is only modestly detrimental to catalysis (6.4-fold at pH 7.0) and does not affect the Mg^{2+} requirement for the reaction within error at pH 7.0 (Chen et al. 2009). This suggests that the lost ion at this position is not critical for catalysis. While an Mg^{2+} interacting directly with the N7 of G1 is not observed in crystal structures of the HDV ribozyme, the crystal structure of the ribozyme postcleavage reveals a metal ion below the plane of G1, in position to interact with the N7 of G1 through its hydration shell (Ferre-D'Amare et al. 1998). The structure of the HDV ribozyme precleavage reveals that there is a ligand to the N7 of G1, but it is not clear if this ligand is a water or a Mg^{2+} ion (Chen et al. 2010). Taken together, it is likely that the pH-sensitive Mg^{2+} ion characterized by Raman spectroscopy and by deazaguanosine substitution at G1 does not interact with phosphate groups and plays, at most, a structural role. This Mg^{2+} ion may occupy the major groove of the P1 and P1.1 helices, where it may be bound in a diffuse fashion. This interpretation is supported by molecular dynamics simulations described below and the constellations of ion and solvent molecules seen in the X-ray crystal structures of the ribozyme (Ferre-D'Amare et al. 1998; Chen et al. 2010). This Mg^{2+} ion will be referred to as the "diffuse Mg^{2+} ion".

8.4.5 Competition Between Hydrated Mg^{2+} Ions and Cobalt Hexammine

The HDV ribozyme is strongly inhibited by cobalt hexamine, $Co(NH_3)_6^{3+}$, in a manner that is competitive with Mg^{2+} (Nakano et al, 2000). $Co(NH_3)_6^{3+}$ is similar in geometry and charge to $Mg(H_2O)_6^{2+}$, and it is often observed to bind to RNAs in sites that are very similar to $Mg(H_2O)_6^{2+}$ binding sites. $Co(NH_3)_6^{3+}$ differs from $Mg(H_2O)_6^{2+}$ in that the NH_3 ligands are exchange inert and cannot participate in

proton-transfer reactions (Basolo and Person 1988; Suga et al. 1998). Inhibition of the HDV ribozyme by $Co(NH_3)_6^{3+}$ suggests that this complex displaces a critical $Mg(H_2O)_6^{2+}$ ion but cannot function in the reaction because of its inability to exchange ligands or participate in proton transfer.

Adding $Co(NH_3)_6^{3+}$ to crystals reveals Raman spectra associated with $Co(NH_3)_6^{3+}$ binding to the RNA (Gong et al. 2009a). Notably, there are no features associated with metal-phosphate ligands. Thus, $Co(NH_3)_6^{3+}$ does not make inner sphere contact with PO_2^- groups, consistent with the exchange-inert nature of the NH_3 ligands. However, $Co(NH_3)_6^{3+}$ is observed to perturb base-ring modes, and in particular there is a distinct feature from a perturbed guanine ring mode. This is consistent with the propensity of $Co(NH_3)_6^{3+}$ to bind in the major groove at tandem G-C and G•U base pairs. $Co(NH_3)_6^{3+}$ appears to bind competitively with the catalytic Mg^{2+} ion; thus, the ring modes of G25 may also be perturbed by $Co(NH_3)_6^{3+}$ binding at this site.

If one of the observed $Co(NH_3)_6^{3+}$ binding sites is within the active site, an energetic interaction between the metal ion and C75 should be observable. Due to the anticooperative coupling of metal binding in the active site and proton binding to C75, C75 is expected to become deprotonated when the active site is loaded with a metal ion. Indeed, deprotonation of cytosine is observed when Mg^{2+} concentrations increase, as described above. Likewise, increasing $Co(NH_3)_6^{3+}$ concentration drives cytosine deprotonation (Gong et al. 2009a), suggesting that a $Co(NH_3)_6^{3+}$ binding site is in proximity to the active site. These results are consistent with a model in which $Co(NH_3)_6^{3+}$ displaces the catalytic Mg^{2+} ion but is unable to participate in catalysis.

Competition between $Co(NH_3)_6^{3+}$ and Mg^{2+} on the HDV ribozyme can be directly probed by comparing spectra containing $Co(NH_3)_6^{3+}$ with and without Mg^{2+}. When $Co(NH_3)_6^{3+}$ or $Mg(H_2O)_6^{2+}$ bind in the major groove, metal-RNA contacts are water-mediated and do not involve contacts to phosphate groups, and this would give no change in the differential near 1,100 cm^{-1} when $Mg(H_2O)_6^{2+}$ displaces $Co(NH_3)_6^{3+}$. The catalytic Mg^{2+} ion, on the other hand, has two ligands to phosphate groups. If an inhibitory $Co(NH_3)_6^{3+}$ ion was replaced with a catalytic Mg^{2+} ion, there would be a net change corresponding to gain of two Mg^{2+}-PO_2^- interactions. Indeed, addition of Mg^{2+} ion to $Co(NH_3)_6^{3+}$-containing crystals results in a differential near 1,100 cm^{-1} and quantitative analysis suggests that between 1 and 1.5 PO_2^--Mg^{2+} interactions are created. This value correlates well with the two phosphate ligands to the catalytic Mg^{2+} ion observed in the recent crystal structure (Chen et al. 2009). Together, the effects of $Co(NH_3)_6^{3+}$ binding on cytosine protonation and PO_2^--Mg^{2+} interactions support localization of one $Co(NH_3)_6^{3+}$ binding site within the active site of the ribozyme, and they show that $Co(NH_3)_6^{3+}$ can displace partially hydrated Mg^{2+} ions in addition to fully hydrated ions. These data further support the model where the Mg^{2+} ion bound at the G25•U20 reverse wobble is the catalytic Mg^{2+} ion.

To summarize, the Raman data support two classes of Mg^{2+} ions in the HDV ribozyme active site: An ion near G1 that binds in a pH-dependent manner and does not interact with a phosphate (the diffuse Mg^{2+} ion), and an ion that is displaced by $Co(NH_3)_6^{3+}$ and interacts with 1 or 2 phosphates (the catalytic Mg^{2+} ion).

8.5 The Catalytic Mechanism of the HDV Ribozyme

8.5.1 Structures Suggest that General Acid and Lewis Acid Catalysis are Both Involved in the Catalytic Mechanism

As described earlier in this chapter (Sect. 8.3.2.1), crystal structures of the HDV ribozyme show that C75 interacts with the 5′-O(H) of G1 in both the precleavage and postcleavage states (Ferre-D'Amare et al. 1998; Chen et al. 2010) (Figs. 8.4a and 8.9). This positioning of C75 implicates it as a general acid in the catalytic reaction. Moreover, solution kinetic experiments and Raman crystallography demonstrate that the pK_a of this base is perturbed by the environment of the HDV ribozyme active site and shifted >2 pH units toward neutrality, which optimizes the base for proton transfer. Additionally, this pK_a couples anticooperatively with Mg^{2+} binding, which provides constraints in proximity of $C75^+$ and an Mg^{2+} ion (see below) and may help drive the reaction (Gong et al. 2007; Nakano et al. 2000; Nakano and Bevilacqua 2007). Further evidence for C75 in proton transfer comes from the Been lab, who demonstrated via Brønsted analysis that the rate of cleavage increases with the basicity of this residue (Shih and Been 2001b; Perrotta et al. 2006). Moreover, in a landmark study, Das and Piccirilli tested whether the mechanism of the cleavage reaction was consistent with C75 serving as a general acid (Das and Piccirilli 2005). They substituted the 5′-oxygen of G1 with a sulfur atom—a good leaving group. When this modification was present, C75 was no longer required for cleavage.

While certain small ribozymes such as the hairpin and VS ribozyme clearly use *only* nucleobase catalysis in their catalytic mechanisms, there is significant evidence that the HDV ribozyme catalysis uses metal ion catalysis in addition to nucleobase catalysis. As described in Sect. 8.4, substrate cleavage is strongly inhibited by $Co(NH_3)_6^{3+}$ (Nakano et al. 2000), a trivalent ion that can often bind in Mg^{2+} binding sites but cannot make inner-sphere interactions with RNA ligands and cannot participate in proton-transfer reactions (Jou and Cowan 1991). Further, Raman crystallography of the HDV ribozyme shows that both Mg^{2+} ion and $Co(NH_3)_6^{3+}$ bind in the active site in a position close enough to C75 to electrostatically "feel" the protonation state of C75 (see above) (Gong et al. 2009a). The structure of the HDV ribozyme in the precleavage state clearly shows an Mg^{2+} ion in the active site that is well defined by electron density. Indeed, our model of the cleavage site dinucleotide suggests that there is a direct interaction between this metal ion and the 2′-hydroxyl nucleophile (Figs. 8.4b and 8.9).

There are multiple mechanisms by which a metal ion could participate in the cleavage reaction (DeRose 2003). By coordinating both the 2′-hydroxyl group of U(−1) and the pro-R_P oxygen of G1, the metal helps to position the nucleophile for in-line attack at the scissile phosphate. Direct coordination of the Mg^{2+} ion to the nucleophile is expected to reduce the pK_a of the nucleophile; thus, Mg^{2+} ion is predicted to serve as a Lewis acid. At present, the destination of the proton lost from the 2′OH of U(−1) is unknown. One early model suggested that an Mg^{2+}-bound

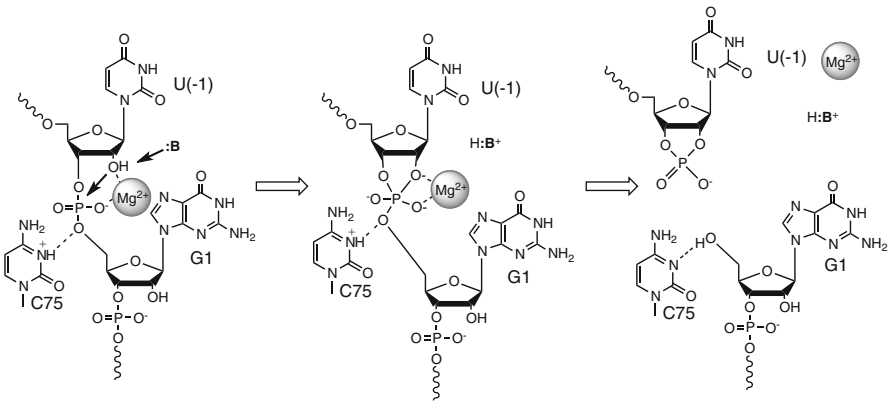

Fig. 8.9 Proposed mechanism for the HDV ribozyme. Shown are general acid and Lewis acid catalysis by the HDV ribozyme via C75 and Mg^{2+}, respectively. The central species could be an intermediate or a transition state. Figure from (Golden 2011) and used with permission

hydroxide ion could serve as a general base and accept the proton from the 2′-hydroxyl group. However, the fact that the reaction is not strongly dependent on the pK_a of the reactive metal ion (e.g. the rate is similar in Ca^{2+}, Mg^{2+}, and Zn^{2+} despite pK_a's of the aqua ions of 12.70, 11.42, and 8.96) makes the role of an Mg^{2+}-bound hydroxide in the rate-pH profile uncertain (Chen et al. 2010).

This leaves us with a mechanism in which two catalytic strategies are at work in the cleavage reaction: general acid catalysis by C75 to stabilize the negatively charged leaving group, and Lewis acid catalysis by the active site Mg^{2+} ion to stabilize the developing negative charge on the 2′-hydroxyl nucleophile. What remains unclear is the identity of the base that accepts the 2′-H of U(−1). It could be solvent water or hydroxide from the surrounding solvent. Alternately, a hydroxide bound to the catalytic metal ion could serve as the general base. Remarkably, both Mg^{2+} and $C75^{+}$ are cationic in their functional forms, hinting at the importance of a negatively charged pocket in the ribozyme's active site.

8.5.2 Three-Channel Model for the Reaction Mechanism

There are multiple pathways to generate the products of the HDV ribozyme reaction (Fig. 8.10). We previously elaborated three different channels for forming product: Channel 1: absence of any divalent ions (but presence of high, 1 M monovalent); Channel 2: presence of a structural divalent ion(s) only; and Channel 3: presence of structural and catalytic divalent ions. This mechanism was developed based largely on examining the reaction rate in the presence of EDTA-buffered reaction channels (Nakano et al. 2001). The difference in observed rates between these

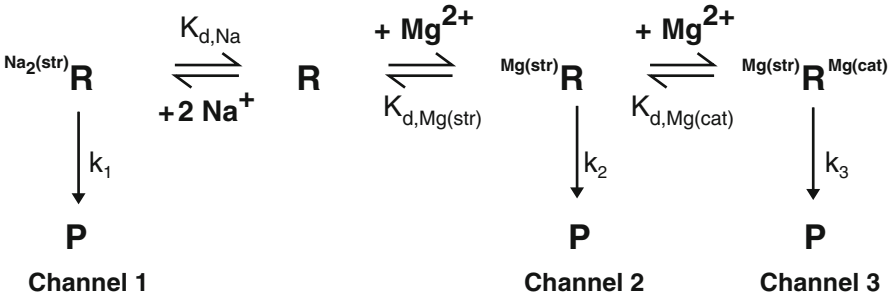

Fig. 8.10 Three-channel model for reaction of the HDV ribozyme. Channel 1 is in the absence of divalent ions but presence of high concentration of monovalent ions to fold the ribozyme. Channel 2 is in the presence of structural divalent ion(s). Channel 3 is in the presence of structural and catalytic divalent ions. Channel 2 is ~125-fold faster than channel 1, and channel 3 is ~25-fold faster than channel 2. Figure from (Nakano et al. 2003) and used with permission

channels is 125-fold for channels 1 and 2, and 25-fold for channels 2 and 3, or an ~3,000 fold increase in rate in going from channel 1 to 3. One of the interesting points is that metal ions contribute more to folding than to chemistry, although the catalytic contribution is nontrivial. A similar 25-fold contribution of divalent ions to chemistry has been found in the hammerhead ribozyme, which also uses a divalent ion in its mechanism (O'Rear et al. 2001; Curtis and Bartel 2001). Thus, both nucleobases and divalent ions can contribute critically to certain small ribozyme reactions.

8.5.3 There Is Unlikely to be Conformational Switching During the Cleavage Reaction

Conformational switching along the cleavage reaction pathway has been suggested on the basis of RNA footprinting experiments, single-molecule FRET experiments, MD simulations, and the crystal structure of the C75U mutant of the HDV ribozyme (Pereira et al. 2002; Ke et al. 2004; Harris et al. 2004; Tinsley et al. 2004; Savochkina et al. 2008; Krasovska et al. 2005). In the reaction model proposed from these data, C75 serves as a general base, and protonation of C75 immediately postcleavage induces a conformational change that drives catalysis. However, comparison of the crystal structures of the HDV ribozyme before and after cleavage suggests a different picture, in which the conformation of the ribozyme active site changes little during catalysis. The discrepancy between the Lewis acid-general acid model (our favored model, described above) and the conformational switching model here is likely the result of two features of the relevant experiments: the pH of the reaction buffer and the C75U mutation, both of which impact the conformational features of the active site.

Many of the solution biochemistry experiments that probed the HDV ribozyme structure were performed at pH 7.5. The pK_a of C75 prior to cleavage under conditions used in these experiments is <6.5 (Gong et al. 2007; Nakano and Bevilacqua 2007). C75 thus exists largely in the deprotonated, inactive state under the conditions used in those studies. This has implications for the structure of the active site because the hydrogen bond between the N3 of C75 and the 5′-hydroxyl leaving group is disrupted, and deprotonation of C75 alters the electrostatics of the active site and increases motions, as described below (Veeraraghavan et al. 2011b). The pK_a of C75 after cleavage is ~4; thus, C75 is also deprotonated at pH 7.5 in the postcleavage state (Luptak et al. 2001). The latter feature allows the hydrogen bond between the N3 of C75 and the 5′-hydroxyl leaving group to be maintained, facilitating the biologically relevant conformation observed in the crystal structure of the ribozyme postcleavage. For these reasons, one expects a conformational difference when comparing biochemical studies of the ribozyme precleavage and postcleavage at pH 7.5, with the former not having hydrogen bonding from C75 to the O5′ of G1 but the latter having it. However, such a conformational change most likely represents a switch that occurs as C75 protonates and the active site of the ribozyme rearranges from a noncatalytic, C75-unprotonated state into a catalytically active C75-protonated state (i.e. a conformational change along the reaction pathway prior to chemistry), not a switch intrinsic to the cleavage reaction (Harris et al. 2004; Tinsley et al. 2004; Pereira et al. 2002; Savochkina et al. 2008).

Likewise, the C75U mutation dramatically changes the structure of the active site (Ke et al. 2004). Although U75, like protonated C75, has a H3 that can serve as a hydrogen bond donor, it lacks both the exocyclic amine and the overall positive charge that are present on a protonated cytosine. Deletion of the exocyclic amine of C75 is detrimental to catalysis (Oyelere et al. 2002). Comparison of the structure of the C75U mutant with the ribozyme pre- or postcleavage reveals why this mutation disrupts the hydrogen-bonding and electrostatic network (discussed above) that helps to organize the active site into a catalytically active conformation. In the C75U mutant, U75 is dislocated out of the pocket that binds C75, and the reverse G25•U20 wobble that helps bind the active site Mg^{2+} ion cannot form (Ke et al. 2004). In the absence of the proper hydrogen bond network, all of the nucleotides in the active site are displaced outward. While an Mg^{2+} ion is present in the active site, its ligands and location are non-native. Thus, it is difficult to make inferences about catalysis from the structure of this inactive mutant. When MD simulations of the wild-type HDV ribozyme sequence are based on the C75U structure, there are insufficient interactions within the active site to maintain a stable $C75^+$ structure in silico, possibly because Mg^{2+} occupies the native site of $C75^+$ and possibly because insufficient sampling takes place. Toggling between alternate conformations is therefore observed (Krasovska et al. 2005). Molecular dynamic simulations on the crystal structure of the ribozyme, when C75 is in its native conformation, trapped precleavage by modification of the 2′-hydroxyl nucleophile (Chen et al. 2010), provide a very different picture of the motions that occur in the ribozyme active site. These results are described in the next section.

8.6 Molecular Dynamics to Assay the Structures, Dynamics, and Electrostatics

Molecular dynamics (MD) simulations have been used to investigate the mechanism of the HDV ribozyme and to clarify several fundamental issues regarding ribozyme catalysis.

8.6.1 Long-Distance Interactions in the HDV Ribozyme

An important general question that has been addressed with MD is how interactions distal from the active site impact catalysis (Veeraraghavan et al. 2010). These MD simulations focused on the interactions between the two protonated cytosines observed in the HDV ribozyme: the catalytic cytosine, C75, and a distal protonated cytosine, C41, which participates in a base triple that has been shown to be important for ribozyme function (Ferre-D'Amare et al. 1998; Ferre-D'Amare and Doudna 2000; Wadkins et al. 2001; Nakano and Bevilacqua 2007). Since the distance between C41 and C75 is ~15 Å, the interaction between these residues is of relatively long range. MD studies were conducted on the postcleavage form of both WT HDV ribozyme and a double mutant (DM) in which the C44-G73 Watson-Crick base pair was mutated to a U-A pair. The DM mutation allows formation of the C41 base triple with neutral rather than the protonated C41 observed in the WT ribozyme. MD trajectories were propagated with both neutral and protonated C41 for the WT and DM ribozymes to determine the impact on the active site. In all four cases, the effects of variations at the C41 base triple on the stability of the active site as observed in the simulations (Veeraraghavan et al. 2010) agreed with the experimental studies on ribozyme activity (Nakano and Bevilacqua 2007). Perturbations of the C41 base triple that resulted in loss of catalytic activity in biochemical activity assays were also observed to disrupt the structure of the active site in the simulations. Overall, these studies suggested that interactions within the ribozyme can communicate over relatively long distances of ~15 Å and that MD simulations of RNA are capable of reproducing such long-range effects.

8.6.2 Roles of the Reverse and Standard G•U Wobbles

MD simulations have also assisted in characterizing the G25•U20 reverse wobble motif in the HDV ribozyme. Beginning with the crystal structure (PDB ID 2CX0) of the postcleavage form of this ribozyme, U20 and G25 were observed to form a stable reverse wobble during equilibration and throughout several independent 25 ns MD trajectories (Veeraraghavan et al. 2010; Veeraraghavan et al. 2011a). Note that this reverse G25•U20 wobble was not present in the crystal structure of the

product; in this crystal structure (PDB ID 2CX0), G25 is *syn*, but the relative angle between U20 and G25 results in long distances of ~4–5 Å between hydrogen bond donors and acceptors. Thus, the MD simulations predicted the existence of the G25•U20 reverse wobble in the postcleavage state. This motif was also observed to form in the postcleavage state in MD simulations conducted by Sponer, Walter, and colleagues (Krasovska et al. 2005). In parallel with the MD studies, the G25•U20 reverse wobble was resolved in a crystal structure of the precleaved state (PDB ID 3NKB), as discussed earlier in this chapter. Furthermore, subsequent analysis of the crystallographic data for the postcleavage state indicated that the G25•U20 reverse wobble is compatible with the diffraction data for the product state as well (Veeraraghavan et al. 2011a). Thus, in contrast to previous proposals suggesting that conformational switching accompanies HDV ribozyme catalysis (Krasovska et al. 2005), these combined MD and crystallographic studies suggested that the G25•U20 reverse wobble, as well as the rest of the active site, remains intact throughout the catalytic reaction.

Metal ion interactions with both the G25•U20 reverse wobble and the G1•U37 wobble at the cleavage site were examined with MD simulations on precleaved ribozyme (Veeraraghavan et al. 2011a; Veeraraghavan et al. 2011b). The catalytic Mg^{2+} bound to the G25•U20 reverse wobble remained intact during several 25 ns MD trajectories. When the catalytic Mg^{2+} ion was removed from the starting structure, Na^{+} ions from the solvent interacted with the G25•U20 reverse wobble. In support of these computational results, competition between Na^{+} and Mg^{2+} has also been observed crystallographically in the precleaved ribozyme (Veeraraghavan et al. 2011a). Analysis of the radial distribution functions between metal ions and the standard and reverse G•U wobble atoms, as well as the charge isodensity plots in the regions of these wobbles, indicated that the metal ion interactions are qualitatively different at the G1•U37 and G25•U20 wobbles (Fig. 8.11). In particular, the catalytic Mg^{2+} bound to the reverse wobble remained localized and was relatively stationary during the MD trajectories, whereas the Mg^{2+} and Na^{+} ions near the G1•U37 wobble were relatively mobile (Fig. 8.11). Following the terminology of Draper (2004), the catalytic metal ion interaction may be characterized as "chelated" and the metal ion near the G1•U37 wobble may be characterized as "diffuse". Thus, the MD studies complement the metal binding site described by Raman crystallography. These chelated and diffuse metal ion interactions appear to contribute to catalysis and stability, respectively, in the HDV ribozyme.

8.6.3 Electrostatic Calculations of the HDV Ribozyme

Nonlinear Poisson-Boltzmann (NLPB) calculations have provided further insight into the metal ion interactions with the G•U wobbles (Veeraraghavan et al. 2011a; Veeraraghavan et al. 2011b). These NLPB calculations reveal an intensely negatively charged patch near the G25•U20 reverse wobble that is optimal for binding metal ions and shifting the pK_a of the catalytic nucleobase, C75, toward neutrality.

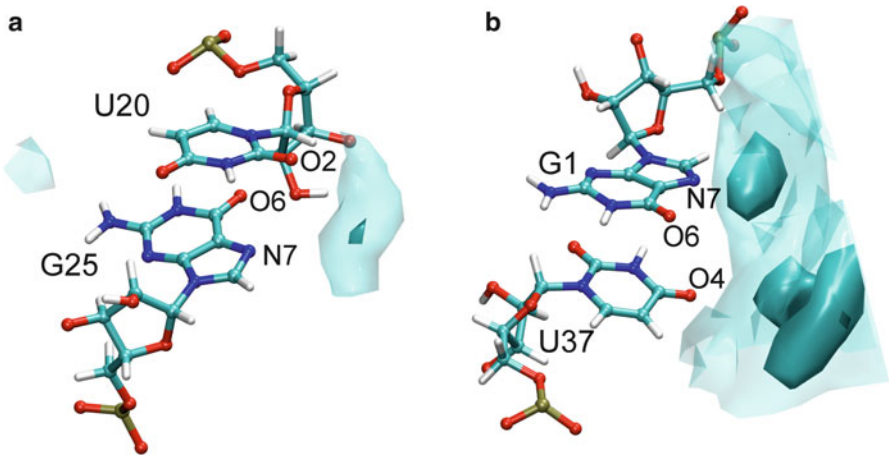

Fig. 8.11 Charge isodensity plots in the regions of the reverse and standard G•U wobbles. (**a**) The reverse G25•U20 wobble and (**b**) the standard G1•U37 wobble. Plots shown here are under conditions of protonated C75 and occupancy of the reverse wobble with Mg^{2+}. Other states of C75 and the reverse wobble are available in (Veeraraghavan et al. 2011b). The darker cyan represents the greatest 30% of the positive charge density, and the lighter cyan represents the greatest 80% of the positive charge density. Figure from (Veeraraghavan et al. 2011b) and used with permission

A negatively charged patch is also observed near the G1•U37 wobble, but the nature of the electrostatic potential is qualitatively different at the reverse and standard G•U wobbles. Specifically, the negatively charged patch is much more negative and more localized at the G25•U20 reverse wobble than at the G1•U37 wobble. These qualitatively different electrostatic potentials are consistent with the more localized and chelated ion near the G25•U20 reverse wobble and the more mobile and diffuse ion near the G1•U37 wobble.

8.6.4 Impact of Mg^{2+} Ion and C75 Protonation on HDV Ribozyme Motion

MD simulations have also been used to investigate the impact of the catalytic Mg^{2+} ion interaction and C75 protonation on the structure and motions of the ribozyme precursor (Veeraraghavan et al. 2011b). The model of the HDV ribozyme in the precleavage state does not undergo significant conformational rearrangements during MD simulations when C75 is protonated and when the active site Mg^{2+} ion is present. The stability of structure in MD simulations provides a nice test of our structural model and this behavior is in contrast to what is observed when simulations are performed on models based on the C75U mutant ribozyme structure (Ke et al. 2004; Krasovska et al. 2005). Protonation of C75 was observed to locally organize the active site, and this facilitates a catalytic mechanism in which $C75^{+}$ acts as a general acid and Mg^{2+} as a Lewis acid, which appears to occur in a concerted fashion

with a divalent ion present at the active site but in a stepwise fashion with monovalent ions present (Ganguly et al. 2011). In particular, deprotonation of C75 was observed to eliminate or weaken important hydrogen-bonding interactions of C75 with G1 and C22. As shown by overlaying thermally averaged structures from two independent MD trajectories with protonated and deprotonated C75 (Fig. 8.12), protonated C75 remains in a reactive alignment, whereas deprotonated C75 does not (Harris et al. 2004; Tinsley et al. 2004; Pereira et al. 2002; Savochkina et al. 2008). In addition, deprotonation of C75 was found to weaken the interaction between the catalytic Mg^{2+} and the nucleophilic O2′ of U-1. Thus, these calculations support the hypothesis that protonation of C75 plays an essential role in aligning the active site for catalysis. Furthermore, the MD simulations indicated that the overall global structure and thermal motions of the ribozyme are not significantly influenced by the catalytic Mg^{2+} interaction or C75 protonation. This analysis, as well as the substantial body of experimental data we have described in this chapter, suggests that the reaction pathway of the HDV ribozyme is dominated by small local motions at the active site rather than large-scale global conformational changes.

8.7 Conclusions

We have taken an integrated approach, combining solution biochemical probing, X-ray crystallography, Raman crystallography, and molecular dynamics, to characterize the structure and catalytic reaction of the HDV ribozyme. This synergistic combination has provided a detailed description of the HDV ribozyme active site and a mechanism of catalysis. The three-dimensional structure of the HDV ribozyme suggests that a protonated $C75^{+}$ and a catalytic Mg^{2+} ion both contribute to the cleavage reaction, with C75 serving as a general acid and the Mg^{2+} ion acting as a Lewis acid. Raman crystallography and solution biochemical analysis demonstrate that the active site environment shifts the pK_a of C75 >2 pH units toward neutrality, enhancing its ability to perform proton-transfer reactions under biologically relevant conditions. Raman crystallography also reveals two types of Mg^{2+} ions in the active site. One ion has direct ligands to phosphate oxygens, binds competitively with $Co(NH_3)_6^{3+}$, and is likely the catalytic Mg^{2+} ion. The second ion, with no direct ligands to phosphate oxygens, appears to bind less tightly and likely interacts with the ribozyme near the G1•U37 base pair. An Mg^{2+} ion in this position is not unambiguously observable in electron density maps and molecular dynamics simulations, suggesting that metal binding in this region may be diffuse. Comparison of the crystal structures pre- and postcleavage suggests that minimal motions are necessary to achieve catalysis. This observation is consistent with molecular dynamics simulations on the ribozyme in both the precleavage and postcleavage states. At the same time, much remains to be learned about how dynamics and electrostatic interactions contribute to the mechanism of the ribozyme. It is our hope that a continued investigation combining kinetics, structure, spectroscopy, and calculations will be greater than the sum of its parts and continue to provide insight into this fascinating catalytic RNA.

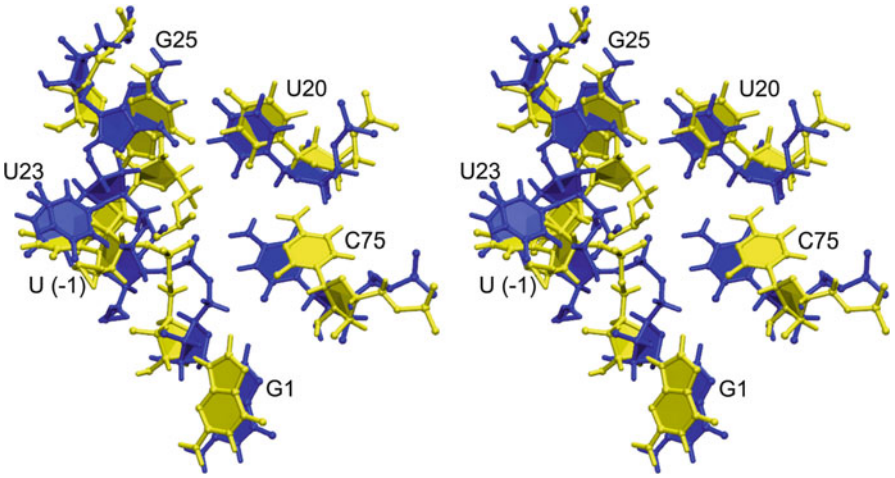

Fig. 8.12 Overlay of thermally averaged structures from trajectories performed on the HDV ribozyme. In the blue structure, C75 was protonated and in the yellow structure C75 was left in the unprotonated state. Deprotonation of C75 results in an increase in the distance between C75(N3) and G1(O5′) from ~3 Å to ~7 Å. Figure from (Veeraraghavan et al. 2011b) and used with permission

Acknowledgments We would like to acknowledge Peter Breen, Trevor Brown, Andrea Cerrone-Szakal, Durga Chadalavada, Elaine Chase, J. Chen, Jui-Hui Chen, Yuanyuan Chen, Eric Christian, Abir Ganguly, Bo Gong, Shu-ichi Nakano, Pallavi Thaplyal, Narayanan Veeraraghavan, and Rieko Yajima for their contributions to this project. These studies were supported by GM095923 (to BLG and PCB), GM81420 (to PRC), and GM56207 (to SHS).

References

Adams PL, Stahley MR, Kosek AB, Wang J, Strobel SA (2004) Crystal structure of a self-splicing group I intron with both exons. Nature 430(6995):45–50

Basolo R, Person R (1988) Mechanisms of inorganic reactions. Wiley, New York

Brown TS, Chadalavada DM, Bevilacqua PC (2004) Design of a highly reactive HDV ribozyme sequence uncovers facilitation of RNA folding by alternative pairings and physiological ionic strength. J Mol Biol 341(3):695–712. doi:10.1016/j.jmb.2004.05.071

Carey PR (1982) Biochemical applications of raman and resonance raman spectroscopies. Academic, New York

Carey PR (2006) Raman crystallography and other biochemical applications of raman microscopy. Ann Rev Phys Chem 57:527–554

Cerrone-Szakal AL, Chadalavada DM, Golden BL, Bevilacqua PC (2008) Mechanistic characterization of the HDV genomic ribozyme: the cleavage site base pair plays a structural role in facilitating catalysis. RNA 14(9):1746–1760. doi:10.1261/rna.1140308

Chadalavada DM, Cerrone-Szakal AL, Bevilacqua PC (2007) Wild-type is the optimal sequence of the HDV ribozyme under cotranscriptional conditions. RNA 13(12):2189–2201. doi:10.1261/rna.778107

Chadalavada DM, Gratton EA, Bevilacqua PC (2010) The human HDV-like CPEB3 ribozyme is intrinsically fast-reacting. Biochemistry 49(25):5321–5330. doi:10.1021/bi100434c

Chadalavada DM, Knudsen SM, Nakano S, Bevilacqua PC (2000) A role for upstream RNA structure in facilitating the catalytic fold of the genomic hepatitis delta virus ribozyme. J Mol Biol 301(2):349–367. doi:10.1006/jmbi.2000.3953

Chadalavada DM, Senchak SE, Bevilacqua PC (2002) The folding pathway of the genomic hepatitis delta virus ribozyme is dominated by slow folding of the pseudoknots. J Mol Biol 317(4):559–575. doi:10.1006/jmbi.2002.5434

Chen JH, Gong B, Bevilacqua PC, Carey PR, Golden BL (2009) A catalytic metal ion interacts with the cleavage Site G.U wobble in the HDV ribozyme. Biochemistry 48(7):1498–1507. doi:10.1021/bi8020108

Chen JH, Yajima R, Chadalavada DM, Chase E, Bevilacqua PC, Golden BL (2010) A 1.9 A crystal structure of the HDV ribozyme precleavage suggests both Lewis acid and general acid mechanisms contribute to phosphodiester cleavage. Biochemistry 49(31):6508–6518. doi:10.1021/bi100670p

Christian EL, Anderson VE, Carey PR, Harris ME (2010) A quantitative Raman spectroscopic signal for metal-phosphodiester interactions in solution. Biochemistry 49(13):2869–2879. doi:10.1021/bi901866u

Cochrane JC, Lipchock SV, Strobel SA (2007) Structural investigation of the GlmS ribozyme bound to Its catalytic cofactor. Chem Biol 14(1):97–105. doi:10.1016/j.chembiol.2006.12.005

Curtis EA, Bartel DP (2001) The hammerhead cleavage reaction in monovalent cations. RNA 7(4):546–552

Das SR, Piccirilli JA (2005) General acid catalysis by the hepatitis delta virus ribozyme. Nat Chem Biol 1(1):45–52. doi:10.1038/nchembio703

DeRose VJ (2003) Metal ion binding to catalytic RNA molecules. Curr Opin Struct Biol 13(3):317–324

Draper DE (2004) A guide to ions and RNA structure. RNA 10(3):335–343

Duguid J, Bloomfield VA, Benevides J, Thomas GJ Jr (1993) Raman spectroscopy of DNA-metal complexes. I. Interactions and conformational effects of the divalent cations: Mg, Ca, Sr, Ba, Mn, Co, Ni, Cu, Pd, and Cd. Biophys J 65(5):1916–1928. doi:10.1016/S0006-3495(93)81263-3

Eickbush DG, Eickbush TH (2010) R2 retrotransposons encode a self-cleaving ribozyme for processing from an rRNA cotranscript. Mol Cell Biol 30(13):3142–3150. doi:10.1128/MCB.00300-10

Emilsson GM, Nakamura S, Roth A, Breaker RR (2003) Ribozyme speed limits. RNA 9(8):907–918

Fauzi H, Kawakami J, Nishikawa F, Nishikawa S (1997) Analysis of the cleavage reaction of a trans-acting human hepatitis delta virus ribozyme. Nucleic Acids Res 25(15):3124–3130

Fedor MJ (2009) Comparative enzymology and structural biology of RNA self-cleavage. Annu Rev Biophys 38:271–299. doi:10.1146/annurev.biophys.050708.133710

Feig AL, Uhlenbeck OC (1999) The role of metal ions in RNA biochemistry. In: Gestlend R, Cech T, Atkins J (eds) The RNA World, 2nd edn. Cold Spring Harbor Laboratory Press, Cold Spring Harber, NY, pp 287–319

Ferre-D'Amare AR (2011) Use of a coenzyme by the glmS ribozyme-riboswitch suggests primordial expansion of RNA chemistry by small molecules. Philos Trans R Soc Lond B Biol Sci 366(1580):2942–2948. doi:10.1098/rstb.2011.0131

Ferre-D'Amare AR, Doudna JA (2000) Crystallization and structure determination of a hepatitis delta virus ribozyme: Use of the RNA-binding protein U1A as a crystallization module. J Mol Biol 295(3):541–556

Ferre-D'Amare AR, Zhou KH, Doudna JA (1998) Crystal structure of a hepatitis delta virus ribozyme. Nature 395(6702):567–574

Frederiksen JK, Piccirilli JA (2009) Identification of catalytic metal ion ligands in ribozymes. Methods 49(2):148–166. doi:10.1016/j.ymeth.2009.07.005

Ganguly A, Bevilacqua PC, Hammes-Schiffer S (2011) Quantum Mechanical/Molecular Mechanical Study of the HDV Ribozyme: Impact of the Catalytic Metal Ion on the Mechanism. J Phys Chem Lett 2(22):2906–2911. doi:10.1021/jz2013215

Golden BL (2011) Two distince catalytic strategies in the HDV ribozyme cleavage reaction. Biochemistry 50(44):9424–9433

Golden BL, Kim H, Chase E (2005) Crystal structure of a phage twort group I ribozyme-product complex. Nat Struct Mol Biol 12(1):82–89

Gong B, Chen JH, Bevilacqua PC, Golden BL, Carey PR (2009a) Competition between Co(NH(3)(6)3+ and inner sphere Mg2+ ions in the HDV ribozyme. Biochemistry 48(50):11961–11970. doi:10.1021/bi901091v

Gong B, Chen JH, Chase E, Chadalavada DM, Yajima R, Golden BL, Bevilacqua PC, Carey PR (2007) Direct measurement of a pK(a) near neutrality for the catalytic cytosine in the genomic HDV ribozyme using Raman crystallography. J Am Chem Soc 129(43):13335–13342. doi:10.1021/ja0743893

Gong B, Chen JH, Yajima R, Chen Y, Chase E, Chadalavada DM, Golden BL, Carey PR, Bevilacqua PC (2009b) Raman crystallography of RNA. Methods 49(2):101–111. doi:10.1016/j.ymeth.2009.04.016

Gong B, Chen Y, Christian EL, Chen JH, Chase E, Chadalavada DM, Yajima R, Golden BL, Bevilacqua PC, Carey PR (2008) Detection of innersphere interactions between magnesium hydrate and the phosphate backbone of the HDV ribozyme using Raman crystallography. J Am Chem Soc 130(30):9670–9672. doi:10.1021/ja801861s

Gong B, Klein DJ, Ferre-D'Amare AR, Carey PR (2011) The glmS Ribozyme Tunes the Catalytically Critical pK(a) of Its Coenzyme Glucosamine-6-phosphate. J Am Chem Soc 133(36):14188–14191. doi:10.1021/ja205185g

Guerrier-Takada C, Gardiner K, Marsh T, Pace N, Altman S (1983) The RNA moiety of ribonuclease P is the catalytic subunit of the enzyme. Cell 35(3 Pt 2):849–857

Guo F, Gooding A, Cech TR (2004) Structure of the tetrahymena ribozyme: Base triple sandwhich and metal ion at the active site. Mol Cell 16(3):351–362

Guo M, Spitale RC, Volpini R, Krucinska J, Cristalli G, Carey PR, Wedekind JE (2009) Direct Raman measurement of an elevated base pKa in the active site of a small ribozyme in a precatalytic conformation. J Am Chem Soc 131(36):12908–12909. doi:10.1021/ja9060883

Harris DA, Tinsley RA, Walter NG (2004) Terbium-mediated footprinting probes a catalytic conformational switch in the antigenomic hepatitis delta virus ribozyme. J Mol Biol 341(2):389–403. doi:10.1016/j.jmb.2004.05.074

Isambert H, Siggia ED (2000) Modeling RNA folding paths with pseudoknots: application to hepatitis delta virus ribozyme. Proc Natl Acad Sci USA 97(12):6515–6520. doi:10.1073/pnas.110533697

Jou R, Cowan J (1991) Ribonuclease H activation by inert transition-metal complexes. Mechanistic probes for metallocofactors: insights on the metallobiochemistry of divalent magnesium ion J Am Chem Soc 113:6685–6686

Ke A, Zhou K, Ding F, Cate JH, Doudna JA (2004) A conformational switch controls hepatitis delta virus ribozyme catalysis. Nature 429(6988):201–205

Klein DJ, Been MD, Ferre-D'Amare AR (2007) Essential role of an active-site guanine in glmS ribozyme catalysis. J Am Chem Soc 129(48):14858–14859. doi:10.1021/ja0768441

Klein DJ, Ferre-D'Amare AR (2006) Structural basis of glmS ribozyme activation by glucosamine-6-phosphate. Science 313(5794):1752–1756. doi:10.1126/science.1129666

Krasovska MV, Sefcikova J, Spackova N, Sponer J, Walter NG (2005) Structural dynamics of precursor and product of the RNA enzyme from the hepatitis delta virus as revealed by molecular dynamics simulations. J Mol Biol 351(4):731–748. doi:10.1016/j.jmb.2005.06.016

Kruger K, Grabowski PJ, Zaug AJ, Sands J, Gottschling DE, Cech TR (1982) Self-splicing RNA: autoexcision and autocyclization of the ribosomal RNA intervening sequence of Tetrahymena. Cell 31(1):147–157

Kuo MY, Sharmeen L, Dinter-Gottlieb G, Taylor J (1988) Characterization of self-cleaving RNA sequences on the genome and antigenome of human hepatitis delta virus. J Virol 62(12):4439–4444

Long DA (2002) The Raman effect. John Wiley & Sons, Ltd. doi:10.1002/0470845767

Luptak A, Ferre-D'Amare AR, Zhou K, Zilm KW, Doudna JA (2001) Direct pK(a) measurement of the active-site cytosine in a genomic hepatitis delta virus ribozyme. J Am Chem Soc 123(35):8447–8452

Mansy .S, Chu G.Y-H, Ducan RE, Tobias RS (1978). Heavy metal-nucleotide interactions. 12. Competitive reactions in systems of far nudeotides with cis- and trans-diamine platinum (II). Raman difference spectrophatometric determination of the relative nucleophilicity of guanine, cytidine, adenosine and uridine monophosphates as well as the analogous bases in DNA. J Am Chen Soc 100(2): 607–616.

Martick M, Scott WG (2006) Tertiary contacts distant from the active site prime a ribozyme for catalysis. Cell 126(2):309–320. doi:10.1016/j.cell.2006.06.036

Moller MR, Bruck MA, O'Connor T, Armatis FJ, Edward A Jr (1980) Heavy metal-nucleotide interactions. 14. Raman difference spectrophometric studies of competitive reactions in mixtures of four nucleotides with electrophiles. Factors governing selectivity in the binding reaction. J Am Chem Soc 102(14):4589–4598

Nakano S, Bevilacqua PC (2007) Mechanistic characterization of the HDV genomic ribozyme: a mutant of the C41 motif provides insight into the positioning and thermodynamic linkage of metal ions and protons. Biochemistry 46(11):3001–3012. doi:10.1021/bi061732s

Nakano S, Cerrone AL, Bevilacqua PC (2003) Mechanistic characterization of the HDV genomic ribozyme: classifying the catalytic and structural metal ion sites within a multichannel reaction mechanism. Biochemistry 42(10):2982–2994. doi:10.1021/bi026815x

Nakano S, Chadalavada DM, Bevilacqua PC (2000) General acid–base catalysis in the mechanism of a hepatitis delta virus ribozyme. Science 287(5457):1493–1497

Nakano S, Proctor DJ, Bevilacqua PC (2001) Mechanistic characterization of the HDV genomic ribozyme: assessing the catalytic and structural contributions of divalent metal ions within a multichannel reaction mechanism. Biochemistry 40(40):12022–12038

O'Rear JL, Wang S, Feig AL, Beigelman L, Uhlenbeck OC, Herschlag D (2001) Comparison of the hammerhead cleavage reactions stimulated by monovalent and divalent cations. RNA 7(4):537–545

Oyelere AK, Kardon JR, Strobel SA (2002) pK(a) perturbation in genomic Hepatitis Delta Virus ribozyme catalysis evidenced by nucleotide analogue interference mapping. Biochemistry 41(11):3667–3675

Peleg M (1972) A Raman spectroscopic investigation of the magesnium nitrate-water system. J Phys Chem 76:1019–1025

Pereira MJ, Harris DA, Rueda D, Walter NG (2002) Reaction pathway of the trans-acting hepatitis delta virus ribozyme: a conformational change accompanies catalysis. Biochemistry 41(3):730–740

Perrotta AT, Been MD (1991) A pseudoknot-like structure required for efficient self-cleavage of hepatitis delta virus RNA. Nature 350(6317):434–436. doi:10.1038/350434a0

Perrotta AT, Shih I, Been MD (1999) Imidazole rescue of a cytosine mutation in a self-cleaving ribozyme. Science 286(5437):123–126

Perrotta AT, Wadkins TS, Been MD (2006) Chemical rescue, multiple ionizable groups, and general acid–base catalysis in the HDV genomic ribozyme. RNA 12(7):1282–1291. doi:10.1261/rna.14106

Pye CC, Rudolph WW (1998) An ab initio and Raman investigation of magnesium(II) hydration. J Phys Chem A 102(48):9933–9943

Reid CE, Lazinski DW (2000) A host-specific function is required for ligation of a wide variety of ribozyme-processed RNAs. Proc Natl Acad Sci USA 97(1):424–429

Reiter NJ, Osterman A, Torres-Larios A, Swinger KK, Pan T, Mondragon A (2010) Structure of a bacterial ribonuclease P holoenzyme in complex with tRNA. Nature 468(7325):784–789. doi:10.1038/nature09516

Rosenstein SP, Been MD (1990) Self-cleavage of hepatitis delta virus genomic strand RNA is enhanced under partially denaturing conditions. Biochemistry 29(35):8011–8016

Rupert PB, Ferre-D'Amare AR (2001) Crystal structure of a hairpin ribozyme-inhibitor complex with implications for catalysis. Nature 410(6830):780–786

Salehi-Ashtiani K, Luptak A, Litovchick A, Szostak JW (2006) A genomewide search for ribozymes reveals an HDV-like sequence in the human CPEB3 gene. Science 313(5794):1788–1792. doi:10.1126/science.1129308

Salehi-Ashtiani K, Szostak JW (2001) In vitro evolution suggests multiple origins for the hammerhead ribozyme. Nature 414(6859):82–84. doi:10.1038/35102081
Savochkina L, Alekseenkova V, Belyanko T, Dobrynina N, Beabealashvilli R (2008) RNase footprinting demonstrates antigenomic hepatitis delta virus ribozyme structural rearrangement as a result of self-cleavage reaction. BMC Res Notes 1:15. doi:10.1186/1756-0500-1-15
Sharmeen L, Kuo MY, Dinter-Gottlieb G, Taylor J (1988) Antigenomic RNA of human hepatitis delta virus can undergo self-cleavage. J Virol 62(8):2674–2679
Shih IH, Been MD (2001a) Energetic contribution of non-essential 5′ sequence to catalysis in a hepatitis delta virus ribozyme. EMBO J 20(17):4884–4891. doi:10.1093/emboj/20.17.4884
Shih IH, Been MD (2001b) Involvement of a cytosine side chain in proton transfer in the rate-determining step of ribozyme self-cleavage. Proc Natl Acad Sci USA 98(4):1489–1494. doi:10.1073/pnas.98.4.1489
Smith JB, Dinter-Gottlieb G (1991) Antigenomic Hepatitis delta virus ribozymes self-cleave in 18 M formamide. Nucleic Acids Res 19(6):1285–1289
Steitz TA, Steitz JA (1993) A general two-metal-ion mechanism for catalytic RNA. Proc Natl Acad Sci USA 90(14):6498–6502
Suga H, Cowan JA, Szostak JW (1998) Unusual metal ion catalysis in an acyl-transferase ribozyme. Biochemistry 37(28):10118–10125. doi:10.1021/bi980432a
Thomas GJ, Tsuboi M (1993) Laser Raman spectroscopy of nucleic acids. Adv Biophys Chem 3:1–70
Tinsley RA, Harris DA, Walter NG (2004) Magnesium dependence of the amplified conformational switch in the trans-acting hepatitis delta virus ribozyme. Biochemistry 43(28):8935–8945. doi:10.1021/bi049471e
Toor N, Keating KS, Taylor SD, Pyle AM (2008) Crystal structure of a self-spliced group II intron. Science 320(5872):77–82. doi:10.1126/science.1153803
Veeraraghavan N, Bevilacqua PC, Hammes-Schiffer S (2010) Long-distance communication in the HDV ribozyme: insights from molecular dynamics and experiments. J Mol Biol 402(1):278–291. doi:10.1016/j.jmb.2010.07.025
Veeraraghavan N, Ganguly A, Chen JH, Bevilacqua PC, Hammes-Schiffer S, Golden BL (2011a) Metal binding motif in the active site of the HDV ribozyme binds divalent and monovalent ions. Biochemistry 50(13):2672–2682. doi:10.1021/bi2000164
Veeraraghavan N, Ganguly A, Golden BL, Bevilacqua PC, Hammes-Schiffer S (2011b) Mechanistic Strategies in the HDV Ribozyme: Chelated and Diffuse Metal Ion Interactions and Active Site Protonation. J Phys Chem B. doi:10.1021/jp203202e
Vogler C, Spalek K, Aerni A, Demougin P, Muller A, Huynh KD, Papassotiropoulos A, de Quervain DJ (2009) CPEB3 is associated with human episodic memory. Front Behav Neurosci 3:4. doi:10.3389/neuro.08.004.2009
Wadkins TS, Been MD (2002) Ribozyme activity in the genomic and antigenomic RNA strands of hepatitis delta virus. Cellular and molecular life sciences: CMLS 59(1):112–125
Wadkins TS, Perrotta AT, Ferre-D'Amare AR, Doudna JA, Been MD (1999) A nested double pseudoknot is required for self-cleavage activity of both the genomic and antigenomic hepatitis delta virus ribozymes. RNA 5(6):720–727
Wadkins TS, Shih I, Perrotta AT, Been MD (2001) A pH-sensitive RNA tertiary interaction affects self-cleavage activity of the HDV ribozymes in the absence of added divalent metal ion. J Mol Biol 305(5):1045–1055. doi:10.1006/jmbi.2000.4368
Webb CH, Luptak A (2011) HDV-like self-cleaving ribozymes. RNA Biol 8(5)
Webb CH, Riccitelli NJ, Ruminski DJ, Luptak A (2009) Widespread occurrence of self-cleaving ribozymes Science 326(5955):953. doi:10.1126/science.1178084
Wilson DS, Szostak JW (1999) In vitro selection of functional nucleic acids. Annu Rev Biochem 68:611–647. doi:10.1146/annurev.biochem.68.1.611
Wu HN, Lin YJ, Lin FP, Makino S, Chang MF, Lai MM (1989) Human hepatitis delta virus RNA subfragments contain an autocleavage activity. Proc Natl Acad Sci USA 86(6):1831–1835